Stationary wave and surface radiative effects weaken and delay the near-surface response to stratospheric ozone depletion

Chaim I. Garfinkel,[a] Ian White,[a] Edwin P. Gerber,[b] Seok-Woo Son,[c] Martin Jucker,[d]

[a] *The Hebrew University of Jerusalem, Institute of Earth Sciences, Edmond J. Safra Campus, Givat Ram, Jerusalem, Israel*

[b] *Courant Institute of Mathematical Sciences, New York University, New York, USA*

[c] *School of Earth and Environmental Sciences, Seoul National University, Seoul, South Korea*

[d] *Climate Change Research Centre and ARC Centre of Excellence for Climate Extremes, University of New South Wales, Sydney, Australia*

Corresponding author: Chaim I. Garfinkel, The Hebrew University of Jerusalem, Institute of Earth Sciences, Edmond J. Safra Campus, Givat Ram, Jerusalem, Israel, chaim.garfinkel@mail.huji.ac.il.

ABSTRACT: An intermediate complexity moist General Circulation Model is used to investigate the factor(s) controlling the magnitude of the surface impact from Southern Hemisphere springtime ozone depletion. In contrast to previous idealized studies, a model with full radiation is used, which allows focus on the full range of feedbacks between incoming ultraviolet radiation and temperature variations. In addition, the model can be run with a varied representation of the surface, from a zonally uniform aquaplanet to a highly realistic configuration. The model captures the positive Southern Annular Mode response to ozone depletion evident in observations and comprehensive models in December through February. It is shown that while synoptic waves dominate the long-term poleward jet shift, the initial response includes changes in planetary waves which simultaneously moderate the polar cap cooling (i.e., a negative feedback), but also constitute nearly half of the initial momentum flux response that shifts the jet polewards. Enhanced ultraviolet absorption at the surface due to the ozone hole drives an additional negative feedback on the poleward jet shift. The net effect is that stationary waves and surface radiative effects weaken the circulation response to ozone depletion, and also delay the response until summer rather than spring when ozone depletion peaks.

1. Introduction

Antarctic springtime ozone concentrations decreased in the last few decades of the twentieth century due to anthropogenic emissions of chlorofluorocarbons (Solomon et al. 1986), and only recently have begun the slow process of recovery (Weber et al. 2018). Ozone depletion is known to have been the dominant contributor over the late 20th century to a poleward shift of the austral summer Southern Hemisphere (SH) tropospheric midlatitude jet, Southern Annular Mode (SAM), precipitation, and storm tracks, and to have led to an expansion of the summer Hadley Cell (Trenberth and Stepaniak 2002; Gillett and Thompson 2003; Son et al. 2010; Thompson et al. 2011; Kang et al. 2011; Polvani et al. 2011; McLandress et al. 2011; Eyring et al. 2013; Gerber and Son 2014; Gonzalez et al. 2014; Previdi and Polvani 2014; Waugh et al. 2015; Seviour et al. 2017; Son et al. 2018). Over the next ~50 years, ozone recovery is expected to nearly cancel out changes in the tropospheric jet and Hadley Cell that would otherwise be forced by greenhouse gases (Son et al. 2008; Polvani et al. 2011; Arblaster et al. 2011; Barnes and Polvani 2013; Gerber and Son 2014; Banerjee et al. 2020). Despite this clear evidence, the mechanism whereby ozone depletion leads to a downward impact, and the details of how this mechanism governs the magnitude of the impact, are still unclear, e.g. as noted in successive WMO Ozone assessments (World Meteorological Organization 2011, 2014; Karpechko et al. 2018).

This study focuses on two processes thought to be important for the downward impact: radiative effects and the role of planetary vs. synoptic waves. Radiative effects, and in particular reduced downward propagating longwave due to colder stratospheric temperatures, may be important for the tropospheric (Grise et al. 2009) and the surface temperature (Yang et al. 2014) response to ozone depletion. However as noted by Trenberth and Stepaniak (2002) and Previdi and Polvani (2014), the SAM accounts for around half of the observed surface warming over the Antarctic Peninsula, nearly all of the observed cooling over East Antarctica, and much of the warming over Patagonia. In addition, the longwave changes due to a colder stratosphere will be balanced in part by enhanced shortwave downwelling, as UV previously absorbed in the stratosphere can now reach the surface (Chiodo et al. 2017). Regardless of how the tropospheric cooling arises, the role of this tropospheric cooling for the jet shift, as compared to other mechanisms for the downward impact, has not been thoroughly explored in previous work though Chiodo et al. (2017) found the net radiative effect to be weak.

SH stationary waves are dominated by wave-1, even in the troposphere (Garfinkel et al. 2020a), and while SH stationary waves are weaker than their counterparts in the Northern Hemisphere, they contribute roughly half of the heat flux in spring in the lower stratosphere (Kållberg et al. 2005) and contribute to the inter-model spread in the timing of the ozone-hole breakup (Hurwitz et al. 2010). A commonly used model in studies focusing on the mechanism(s) for the surface response to ozone depletion is a dry dynamical core with a flat bottom (e.g. Kushner and Polvani 2004; Sun et al. 2014; Yang et al. 2015; Smith and Scott 2016) allowing for transient planetary waves only, or a highly idealized mountain (Gerber and Polvani 2009; Domeisen et al. 2013). The importance of stationary waves in the SH for a surface response cannot be readily evaluated in such setups by construction. Many of these studies using flat-bottomed models nevertheless conclude that planetary waves are crucial for the surface response. For example, Smith and Scott (2016) find that the response to a stratospheric perturbation is weaker if interactions between planetary- and synoptic-scale waves are suppressed, while Domeisen et al. (2013) find that the jet shifts in the opposite direction if only planetary waves are present, ruling out the possibility that the jet shift occurs purely as a response to changes in the planetary- or synoptic-scale wave fields alone. However the lack of stationary planetary waves in these models resembling those in the SH may lead to a mis-representation of the total impact of planetary waves.

The goals of this study are to answer these two questions:

1. how do changes in UV absorption at the surface (due to the lack of absorption in the stratosphere) affect the timing and intensity of the jet shift?

2. what is the relative role of synoptic vs. planetary waves for the downward impact?

We take advantage of a recently developed intermediate complexity model that can delineate the role of these two effects. First, it can be run alternately with realistic stationary waves or without any zonal asymmetry in the bottom boundary (e.g., topography), and thus clarify the role of stationary waves for the surface response. Second, it can be run alternately with an ozone hole in which surface shortwave feedbacks are present, or with a stratospheric diabatic temperature tendency that mimics the shortwave effects of ozone depletion in the stratosphere only, thus clarifying the role of surface shortwave changes.

After introducing this model in Section 2 and our diagnostics in Section 3, we demonstrate in Section 4 that the model in its most realistic configuration simulates a quantitatively realistic response to ozone depletion, but that the response is significantly stronger in an aquaplanet configuration. We consider two complementary reasons for this effect in Section 5, and then summarize our results and place them in the context of previous work in Section 6.

2. A model of an idealized moist atmosphere (MiMA)

We use the Model of an idealized Moist Atmosphere (MiMA) introduced by Jucker and Gerber (2017), Garfinkel et al. (2020b), and Garfinkel et al. (2020a). This model builds on the aquaplanet models of Frierson et al. (2006), Frierson et al. (2007), and Merlis et al. (2013). Very briefly, the model solves the moist primitive equations on the sphere, employing a simplified Betts-Miller convection scheme (Betts 1986; Betts and Miller 1986), idealized boundary layer scheme based on Monin-Obukhov similarity theory, and a purely thermodynamic (or slab) ocean. An important feature for this paper is that we use a realistic radiation scheme Rapid Radiative Transfer Model (RRTMG) (Mlawer et al. 1997; Iacono et al. 2000), which allows us to explicitly simulate the radiative response to ozone depletion, unlike previous studies using more idealized models with Newtonian cooling. Please see Jucker and Gerber (2017) for more details.

This model can be run alternately as an aquaplanet, or with stationary waves quantitatively similar to those in comprehensive models (Garfinkel et al. 2020b,a). The most realistic configuration of MiMA used in this study has boundary forcings that are identical to those of Garfinkel et al. (2020a), and this configuration is referred to as STAT in the rest of this paper. MiMA has no true land, rather the properties of the surface at gridpoints that are land on Earth are modified to mimic land (Figure 3 of Jucker and Gerber 2017). The net effect is that the STAT configuration includes three sources of zonal asymmetry in the lower boundary: orography, prescribed east-west ocean heat transport, and land-sea contrast (i.e., difference in heat capacity, surface friction, and moisture availability between “ocean" gridpoints and “land" gridpoints). The specifications of these forcings can be found in Garfinkel et al. (2020a). Note that the same albedo value is applied to all wavelengths of incoming solar radiation.

We analyze the response to an identical ozone hole for four different tropospheric configurations: (i) the Southern Hemisphere (SH) of STAT, (ii) the Northern Hemisphere (NH) of STAT (STATNH), (iii) an aquaplanet with albedo of 0.27 globally (including over “Antarctica"), and (iv) and an aquaplanet but in which the albedo over “Antarctica" is increased to 0.8 and elsewhere lowered to 0.23 (as in STAT, see equation A3 of Garfinkel et al. 2020a) to help maintain a similar global mean temperature. We refer to these last two experiments as AQUA27 and AQUA80 in the rest of this paper. The AQUA runs have no stationary waves, but both aquaplanet integrations still include north-south ocean heat transport (Eq. A4 of Garfinkel et al. 2020a). The aquaplanet runs use a mixed-layer depth of 75m everywhere, in contrast to STAT which has a mixed layer depth of 2.5m over "land" and a varying depth for ocean gridpoints (see Eq. A2 of Garfinkel et al. 2020a). The NH STAT configuration is not meant to simulate a boreal winter ozone "hole", either as observed in 1997, 2011 or 2020 (Hurwitz et al. 2011; Manney et al. 2011; Rao and Garfinkel 2020; Lawrence et al. 2020; Rao and Garfinkel 2021) or as in a world avoided scenario (Newman et al. 2009; Garcia et al. 2012). Rather, it explores how the exact same change of ozone impacts the circulation with a very different climatology of stationary (and synoptic) waves.

For all tropospheric configurations, we compare a pair of simulations: (1) a preindustrial simulation forced with the monthly varying climatology of ozone in the CMIP6 ozone specification averaged from 1860 to 1899 (PI simulation; Checa-Garcia et al. 2018; Checa-Garcia 2018); and (2) a simulation forced with the monthly varying climatology of ozone in the CMIP6 ozone specification averaged from 1990 to 1999, which we then further reduce by a factor of 4 between 150hPa and 30hPa and poleward of 65S following:

$$\Phi(\varphi) = 1 - 3/8\left(1 - \tanh\left[\frac{\varphi + 65^\circ}{3^\circ}\right]\right), \tag{1}$$

where φ denotes latitude (ozone hole simulation). This additional reduction in the polar lower stratosphere is intended to capture springs with stronger than average ozone depletion (Previdi and Polvani 2014), and is included to enhance the signal to noise ratio. An experiment without this additional reduction leads to a weaker surface response, which is consistent with previous work that has argued that interannual variability of ozone concentrations can be used to improve the skill of seasonal and subseasonal forecasting (Son et al. 2013; Bandoro et al. 2014; Hendon et al. 2020; Jucker and Goyal 2021). The linearity of the response is discussed in more detail in Section 5c.

The ozone hole runs branch from October 1st of the last 65 years of the respective preindustrial control runs, and are then integrated for at least 150 days. The results are shown in terms of the difference between the ozone hole simulation and the PI simulation (ozone hole - PI), though all conclusions are just as applicable to ozone recovery. The net effect on ozone is shown in Figure

1abc, which show days 1 to 30 (October), 31 to 70 (November and early December), and 71 to 120 (rest of December and January). The ozone perturbation is evident throughout the spring and decays in early summer. In the polar lower stratosphere, more than 90% of the preindustrial ozone is locally depleted, and this reduction is within the range of realistic values (Solomon et al. 2005; Previdi and Polvani 2014). Ozone actually increases slightly in the upper stratosphere in summer due to dynamical feedbacks (Stolarski et al. 2006).

In order to isolate the role of surface shortwave absorption, and also to more cleanly connect our results to studies using dry models with an imposed diabatic heating (Kushner and Polvani 2004; Sheshadri and Plumb 2016; White et al. 2020), we also performed simulations in which a diabatic heating perturbation is imposed in the lower stratosphere. Our goal is to match the stratospheric diabatic heating perturbation due to ozone, and thus we show in Figure 1d-f the diabatic heating perturbation due to the reduced ozone as computed by the model. The diabatic heating rate is ~ -0.5K/day in the polar lower stratosphere. The upper stratospheric diabatic tendency is due to the dynamically induced warming resulting in enhanced longwave emission (Manzini et al. 2003; McLandress et al. 2010; Orr et al. 2012a). Motivated by this, we impose a diabatic perturbation between 150hPa and 30hPa of the form of equation 1, and hold it constant in time with no seasonality. The effect of this diabatic heating perturbation is explored both for a diabatic heating perturbation similar in magnitude and location to the one due to ozone depletion (peaking at -0.5K/day; DIAB simulation) and also a factor of five larger (peaking at -2.5K/day; DIAB5x simulation).

Table 1 summarizes all experiments included in this paper. For all integrations, the model is forced with CO_2 concentrations fixed at 390ppmv and seasonally varying solar insolation. All simulations in this paper were run with a triangular truncation at wavenumber 42 (T42) with 40 vertical levels.

3. Diagnostics

The role of synoptic and planetary waves in driving the poleward jet shift is diagnosed using the Eulerian mean zonal momentum budget:

Table 1. MiMA Experiments, with "Y" indicating a forcing is on and "N" indicating a forcing is off. For ozone, we compare a "preindustrial" simulation using ozone concentrations from the CMIP6 read-in file over the years 1860-1899 to a simulation using ozone concentrations from the CMIP6 read-in file over the years 1990-1999, which were then modified in the Antarctic lower stratosphere (see section 2) to capture a deeper ozone hole evident in some years. The jet latitude is included for November in the SH.

Table: MiMA Model experiments

	surface zonal structure	"Antarctica" albedo	"Antarctica" mixed layer	Nov jet latitude
STAT, hole-PI	Y	0.8	2.5m	50.1S
AQUA80, hole-PI	N	0.8	75m	46.5S
AQUA27, hole-PI	N	0.27	75m	43.1S
STATNH, hole-PI	Y	0.8	2.5m	
STAT, diab-PI	Y	0.8	2.5m	50.1S
AQUA80, diab-PI	N	0.8	75m	46.5S
STAT, diab5x-PI	Y	0.8	2.5m	50.1S
AQUA80, diab5x-PI	N	0.8	75m	46.5S

$$
\begin{aligned}
\frac{\partial \overline{u}}{\partial t} = &-\underbrace{\left(\frac{1}{a\cos^2\varphi}\frac{\partial}{\partial \varphi}(\cos^2\varphi\overline{u'v'}_{k\leq 3}) + \frac{1}{\rho_0}\frac{\partial}{\partial z}(\rho_0\overline{u'w'}_{k\leq 3})\right)}_{eddy_{1-3}} \\
&-\underbrace{\left(\frac{1}{a\cos^2\varphi}\frac{\partial}{\partial \varphi}(\cos^2\varphi\overline{u'v'}_{k>3}) + \frac{1}{\rho_0}\frac{\partial}{\partial z}(\rho_0\overline{u'w'}_{k>3})\right)}_{eddy_{4+}} \\
&+\underbrace{f\overline{v}}_{\text{fv}} - \underbrace{\left(\overline{w}\frac{\partial \overline{u}}{\partial z} + \frac{\overline{v}}{a\cos\varphi}\frac{\partial}{\partial \varphi}(\overline{u}\cos\varphi)\right)}_{\text{advect}} + \overline{X} + \text{res} \qquad (2)
\end{aligned}
$$

(e.g., Andrews et al. 1987; Hitchcock and Simpson 2016) where the acceleration of the zonal-mean zonal wind on the left hand side is contributed to by processes associated with (from left to right on the right hand side): eddy momentum flux convergence due to planetary waves ($eddy_{1-3}$), eddy momentum flux convergence due to synoptic waves ($eddy_{4+}$), Coriolis torques acting on the meridional motion (fv), mean flow momentum advection (advect), and parameterised processes including the zonal wind tendency due to vertical and horizontal diffusion and gravity-wave drag in the model ($\overline{X}$). All variables follow standard notation (e.g., see Andrews et al. 1987). The final term (res) is the budget residual and is contributed to by issues associated with sampling and truncation errors.

The Southern Annular mode (SAM) and the e-folding timescale of the corresponding principle component timeseries is computed following the methodology of Baldwin et al. (2003) and Gerber et al. (2008). Jet latitude is computed by fitting the 850hPa zonal mean zonal wind near the jet maxima (as computed at the model's T42 resolution) to a second order polynomial, and then evaluating the polynomial at a meridional resolution of $0.12°$. The latitude of the maximum of this polynomial is the jet latitude (Garfinkel et al. 2013a).

4. The response to an identical ozone perturbation in STAT and in AQUA80

We begin by showing that in the STAT configuration of MiMA, ozone loss leads to impacts similar to those shown in previous works using reanalysis or comprehensive models. Figure 1ghi shows the temperature response to reduced ozone. Temperatures in the polar lower stratosphere gradually decrease over the first two months and reach -15K by November, and the anomaly propagates downward to near the tropopause in late December (Figure 1i). This cooling is similar to that observed during years with a particularly strong ozone hole relative to 1960s conditions (Randel et al. 2009; Previdi and Polvani 2014). The zonal wind response is shown in Figure 1jkl, and captures the response evident in reanalysis, CMIP, and CCMI data (Previdi and Polvani 2014; Son et al. 2018). Changes in 500hPa geopotential height also resemble the canonical SAM pattern (Figure 2bc, Kidson 1988; Thompson and Wallace 2000; Thompson et al. 2011) with lower heights in subpolar latitudes and higher heights between 40S and 50S. The model also simulates the precipitation response to ozone depletion (unlike dry models used in many mechanistic studies). Figure 2def shows an increase in precipitation over Southeastern Australia and Southeastern South America and drying over New Zealand (in agreement with observed trends; Hendon et al. 2007; Ummenhofer et al. 2009; Gonzalez et al. 2014).

The increase in subpolar zonal wind peaks near day 90 at 70hPa (January 1st; Figure 3a), though higher in the stratosphere the response peaks earlier, and is followed by a zonal wind and SAM response in the troposphere (Figure 3b for 850hPa wind and 3c for geopotential height). While a tropospheric response begins to develop in November, the response peaks in January and persists into February in agreement with previous work.

Encouraged by the quantitative accuracy of the response in the most realistic configuration, we now take advantage of the flexibility of the idealized model in order to understand the role of stationary waves and shortwave effects for the surface response. As discussed in Section 2, the same ozone perturbation has also been imposed in two aquaplanet configurations of the model (differing only in the polar albedo) and in the Northern Hemisphere. We begin with the aquaplanet configuration with a polar albedo of 0.8 (AQUA80), as this turns out to be the tropospheric configuration with the largest surface response to ozone depletion. Even though the ozone perturbations are identical, the wind response (Figure 1, bottom row) is larger in AQUA80. The difference in zonal wind response between the two configurations is statistically significant at the 5% level after day 45 in both the stratosphere and troposphere (Figure 4). The geopotential height response in the troposphere is more than twice as large in AQUA80 than in STAT (Figure 2abc vs 5abc and Figure 3c vs. 6c), and the precipitation response is also stronger although less regionally focused due to the lack of Antarctica orography (Figure 5def). The difference in response is evident both in November and in December/January (Figure 6b and Figure 7abc).

5. Why the stronger response for AQUA80?

STAT and AQUA80 differ in two aspects: AQUA80 has a mixed layer depth of 75m over Antarctica while STAT has a mixed layer depth of only 2.5m. Even though both configurations have an albedo of 0.8 over Antarctica, this difference in the mixed-layer depth leads to a polar surface warming in STAT of nearly 1K [1], but a 4K cooling occurs in AQUA80 consistent with dynamically induced colder temperatures associated with a positive SAM (Figure 7d and contrast Figure 5ghi and 2ghi). The warming in STAT extends from the surface into the mid-troposphere (Figure 8b) and the difference between STAT and AQUA80 is statistically significant (Figure 8c). Section 5a isolates the impact of this surface shortwave response for the circulation response.

These integrations also differ in their representation of stationary waves: AQUA80 clearly has none. Section 5b considers the impact of stationary waves for the response.

[1]Note that observations indicate a cooling over Antarctica, a feature STAT misses, likely because our albedo is identical for visible/UV and near-IR, while in reality the albedo is approximately 0.97 for visible/UV but much lower for near-IR (Wiscombe and Warren 1980; Grenfell et al. 1994; Gardner and Sharp 2010; Chiodo et al. 2017).

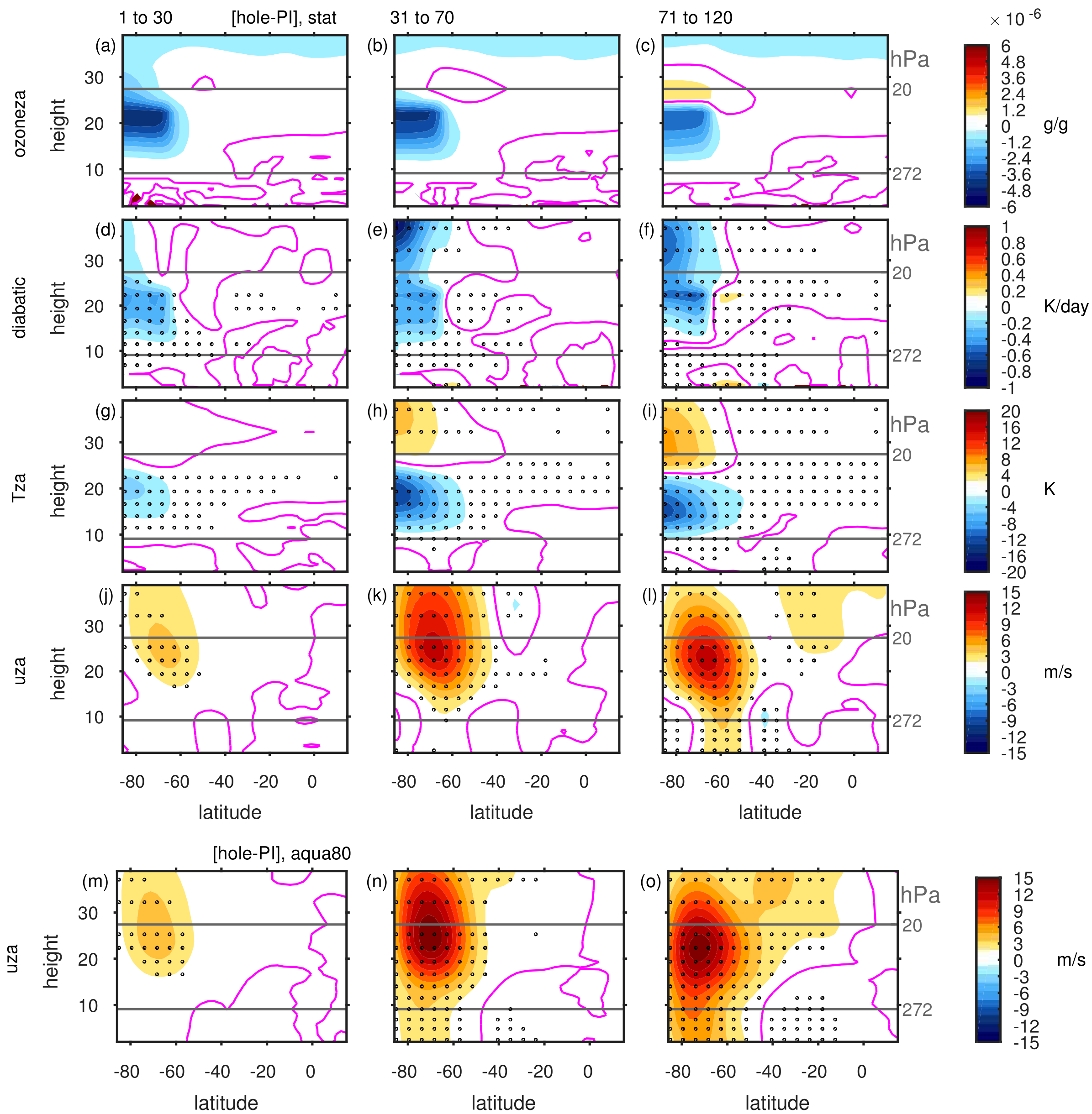

FIG. 1. Zonal-mean responses to ozone loss [i.e., ozone hole minus preindustrial (PI)] in the most realistic configuration, STAT, in (left) days 1-30 after branching, i.e. October; (middle) days 31 to 70, i.e. November and December 1-10; (right) days 71 to 120, i.e. December 11 through January 30. (a-c) ozone perturbation; (d-f) diabatic heating rate computed as the sum of the temperature tendency due to longwave, shortwave, and latent heat release; (g-i) temperature; (j-l) zonal wind. The bottom row is as in (j) through (l) but for an aquaplanet configuration with "Antarctic" albedo=0.8. Stippling indicates anomalies statistically significant at the 95% level. The zero contour is shown in magenta.

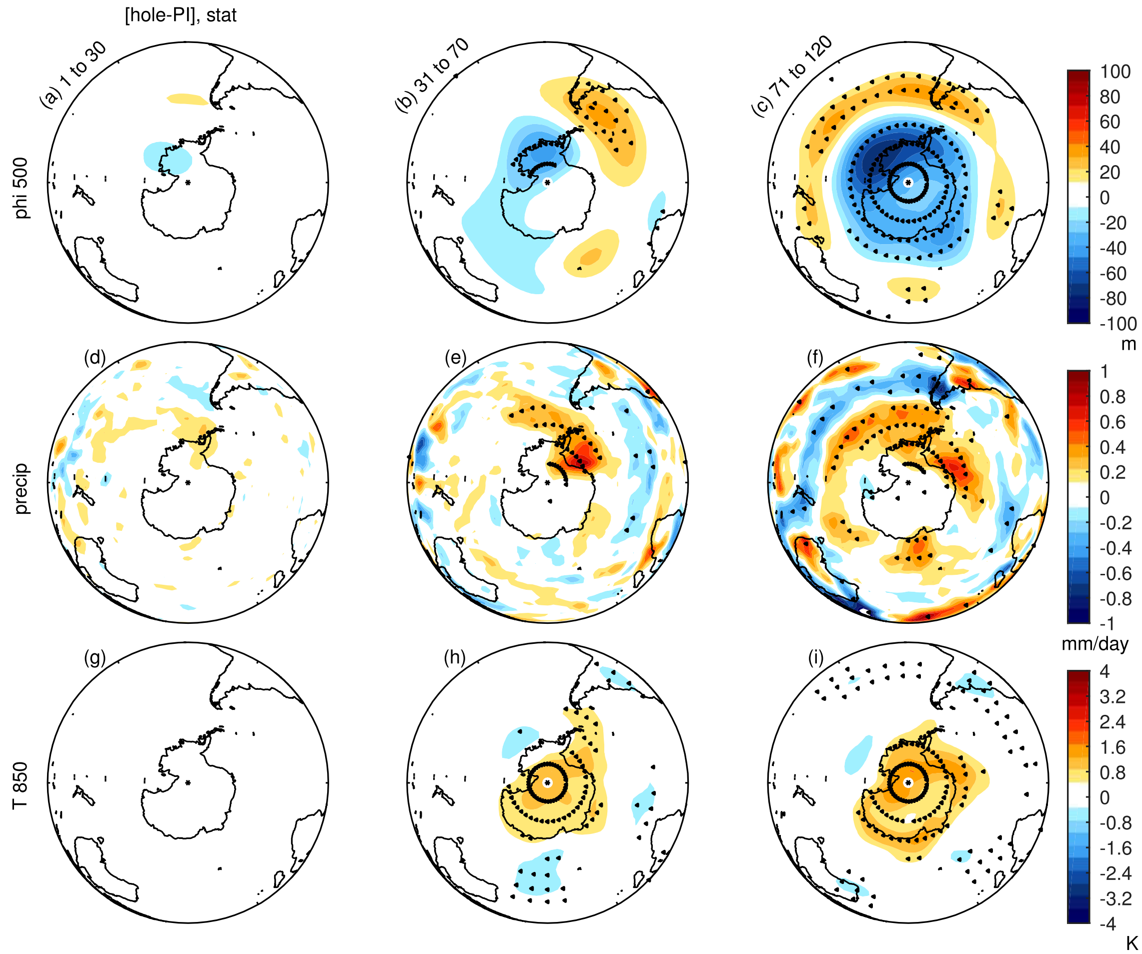

FIG. 2. Map view of ozone loss response (ozone hole - PI) in the most realistic configuration in (left) days 1-30 after branching, i.e. October; (middle) days 31 to 70; (right) days 71 to 120. (a-c) geopotential height at 500hPa; (d-f) precipitation; (g-i) temperature at 850hPa. Stippling indicates anomalies statistically significant at the 95% level.

a. A shortwave negative feedback for the jet response

As discussed above, the near-surface of Antarctica warms for STAT and cools for AQUA80 due to differences in surface processes (Figure 8c). An ozone hole allows more UV to reach the surface, and in STAT a warmer near-surface tropospheric polar cap leads to higher heights throughout the column, including at 500hPa (Figure 5abc and 2abc) and above. The net effect is that the meridional gradient in geopotential is more extreme in AQUA80 than in STAT, and the jet shift is therefore stronger. The hypsometric equation can be used to quantify the contribution of changes in temperature below 500hPa versus those above 500hPa for changes in stratospheric

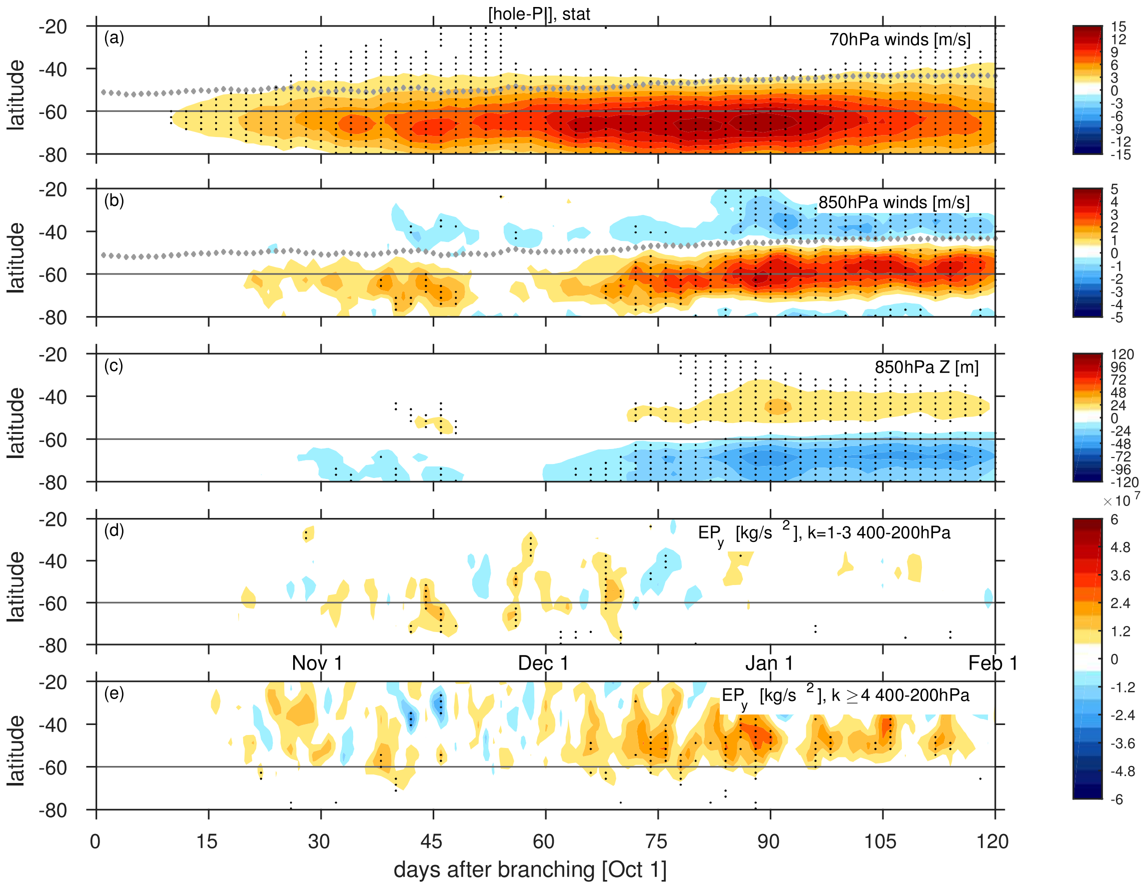

FIG. 3. Development and downward propagation of the response to the ozone perturbation in the most realistic configuration. (a) 70hPa zonal wind; (b) 850hPa zonal wind; (c) 850hPa polar cap geopotential height; upper tropospheric meridional Eliassen-Palm flux due to (d) planetary and (e) synoptic waves. The tropospheric jet latitude is shown in (a) and (b) with gray diamonds. Stippling indicates anomalies statistically significant at the 95% level.

polar cap height (and therefore subpolar zonal wind). Even in the lower stratosphere approximately 30% of the difference in polar cap height between STAT and AQUA80 is due to changes in lower tropospheric temperature. The net effect is that the polar surface warming in STAT in isolation would lead to an equatorward jet shift which cancels part of the ozone-induced poleward shift, and hence is a negative feedback. Conversely, a polar cap cooling due to e.g., longwave effects can help drive a poleward shift (consistent with Grise et al. 2009). However, in our STAT simulation this longwave effect is weaker than the shortwave effect.

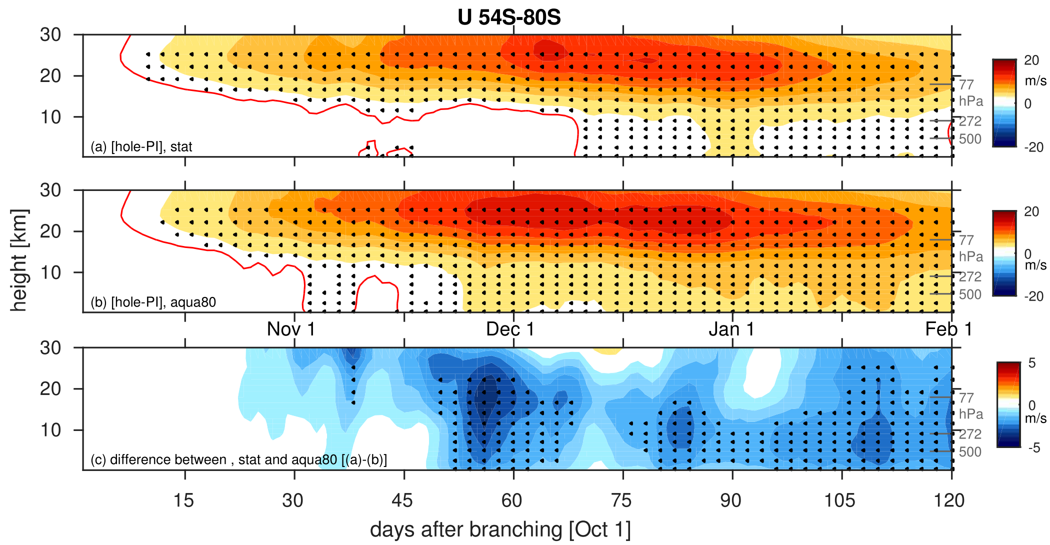

FIG. 4. Evolution of zonal wind from 54S to 80S for the [ozone hole-PI] runs with (a) realistic stationary waves, (b) an aquaplanet, with “Antarctic" albedo equal to 0.8. (c) difference between (a) and (b). The contour interval is 2m/s in (a) and (b) and 0.5m/s in (c). The 1m/s contour is indicated in red in (a) and (b). Stippling indicates anomalies statistically significant at the 95% level.

The comparison of STAT to AQUA80 includes both this shortwave effect and also the stationary wave effect to be discussed shortly, and in order to isolate the surface shortwave effect, we perform an additional aquaplanet integration with polar albedo of 0.27 (AQUA27). AQUA80 and AQUA27 differ only in the specification of albedo, and hence by comparing them we can focus on the effects of shortwave radiation reaching the surface. In AQUA27, surface temperatures rise over Antarctica (Figure 7d) due to enhanced ultraviolet absorption, opposite to AQUA80. The stratospheric zonal wind response is weaker (Figure 7b and Figure 9), and consistent with a weaker stratospheric response and with lower tropospheric warming, the tropospheric wind response is weaker in AQUA27 than in AQUA80 (Figure 7c, and Figure 9). This weakening of the response in AQUA27 vs. AQUA80 occurs even as the jet latitude is further equatorward and the e-folding timescale of the SAM is slightly larger in AQUA27 (Figure 7, Table 1), two factors which would be expected to lead to a stronger response (Garfinkel et al. 2013b).

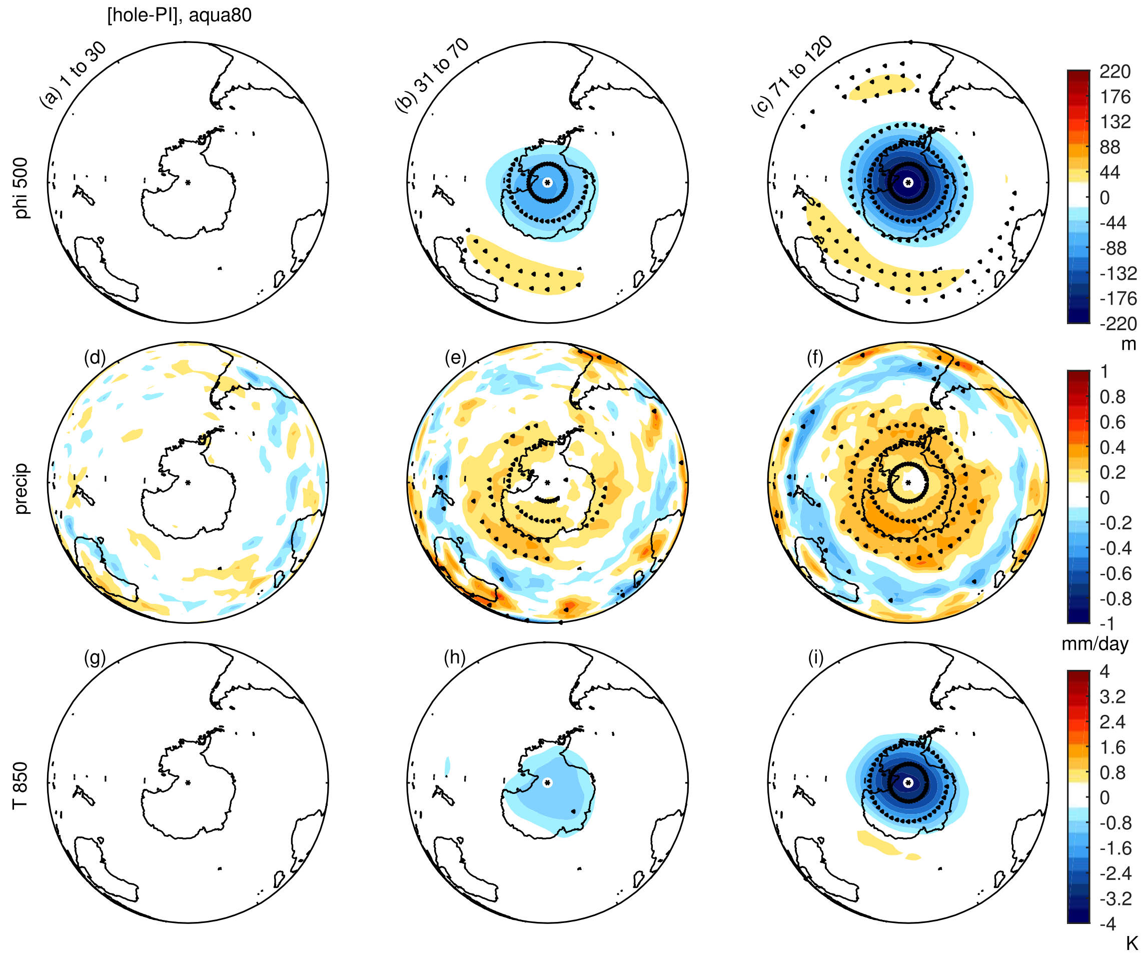

FIG. 5. As in Figure 2 but for an aquaplanet configuration with "Antarctic" albedo=0.8. Note that the color scale for the top row differs from Figure 2.

b. A stationary wave negative feedback for the jet response

In addition to this surface shortwave effect, there is an additional cause for the differences between AQUA80 and STAT in the intensity of the ozone-induced jet shift. Adding stationary waves leads to less of a cooling of the polar lowermost stratosphere (Figure 7a and Figure 8c) even though the ozone perturbation is identical. This difference in response to an identical ozone perturbation occurs because the strengthened vortex in late fall and early summer due to ozone depletion favors more upward wave propagation, and the subsequent enhanced wave convergence within the stratosphere leads to dynamical warming of the polar cap via downwelling of the transformed Eulerian mean vertical wind. This cancels a part of the radiatively driven cooling near the tropopause (not shown,

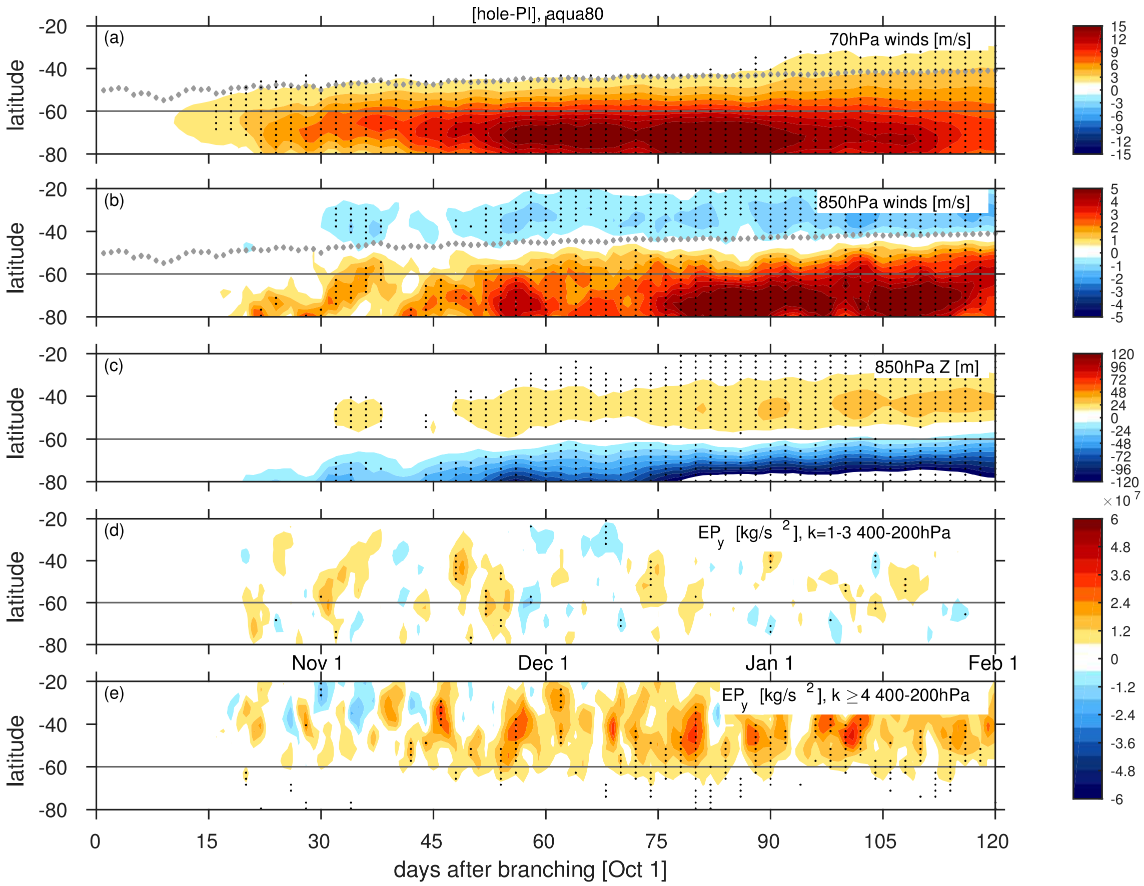

FIG. 6. As in Figure 3 but for aquaplanet with “Antarctic" albedo=0.8.

but as in Manzini et al. 2003; Li et al. 2010; McLandress et al. 2010; Orr et al. 2012a). However this increase in upward propagating waves is more dramatic in the presence of stronger wave forcing from below, and in STAT these upward propagating waves are indeed stronger due to the presence of stationary waves. We demonstrate this effect in Figure 7e, which shows the vertical component of the Eliassen-Palm flux at 40hPa, though other levels in the mid- and lower- stratosphere show a similar response. In STAT, an ozone hole leads to increased upward wave flux by late October, and the anomaly stays positive throughout the duration of the run. The increase in AQUA80 is weaker however, and the difference between STAT and AQUA80 is statistically significant between days 75 and 90. The net effect is a warmer polar stratosphere in STAT (Figure 8c). Hence, stationary waves act as a negative feedback on the surface and stratospheric response to ozone, acting to partially offset the ozone-induced cooling and poleward jet shift.

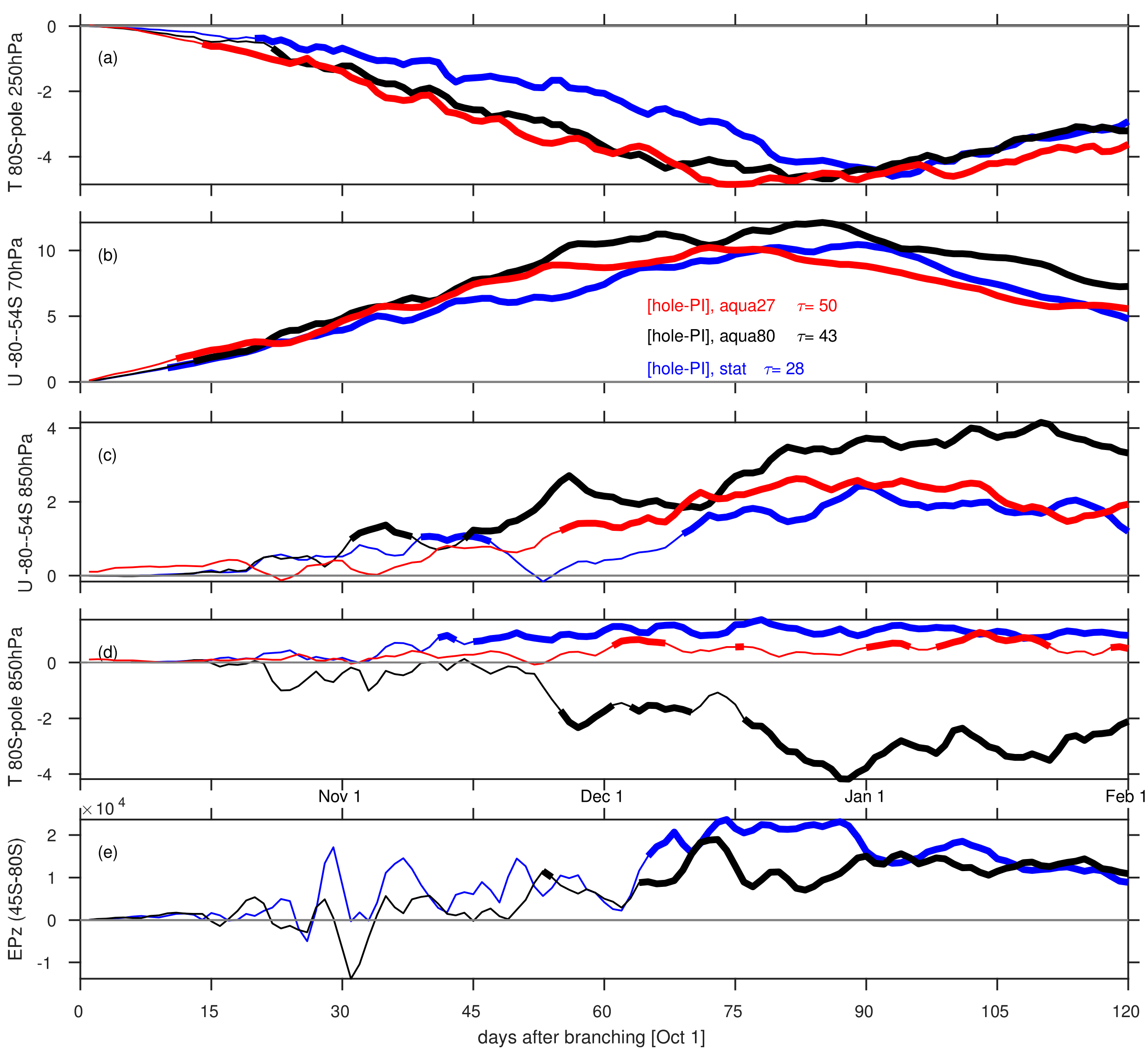

FIG. 7. Summary of responses to ozone depletion [ozone hole-PI]. (a) polar cap temperature at 250hPa [K]; area-weighted average of zonal wind from 80S to 55S [m/s] at (b) 70hPa and (c) 850hPa; (d) polar cap temperature at 850hPa [K]; (e) vertical component of the EP flux at 40hPa area-weighted average from 80S to 45S [kg/s^2]. Blue line is for most realistic configuration. Red line is for an aquaplanet, with “Antarctic" albedo equal to 0.27. Black line is for an aquaplanet, with “Antarctic" albedo equal to 0.8. A thick line indicates regions in which a null hypothesis of no effect can be rejected at the 95% confidence level. The legend also includes the SAM e-folding timescale of each configuration in January.

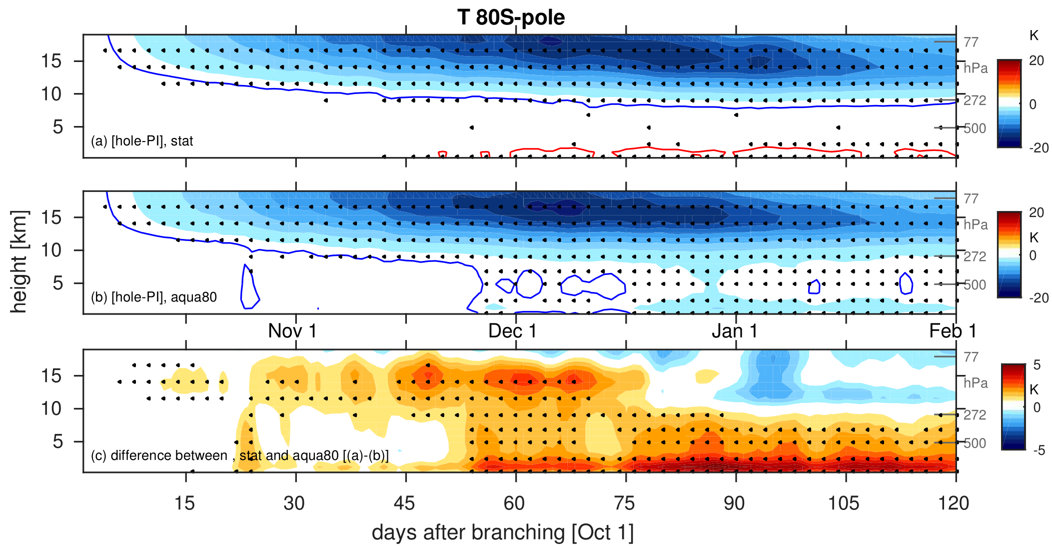

FIG. 8. Evolution of polar cap T for the [ozone hole-PI] runs with (a) realistic stationary waves, (b) an aquaplanet, with “Antarctic" albedo equal to 0.8. (c) difference between (a) and (b). The -1K(1K) contour is indicated in blue(red) in (a) and (b).

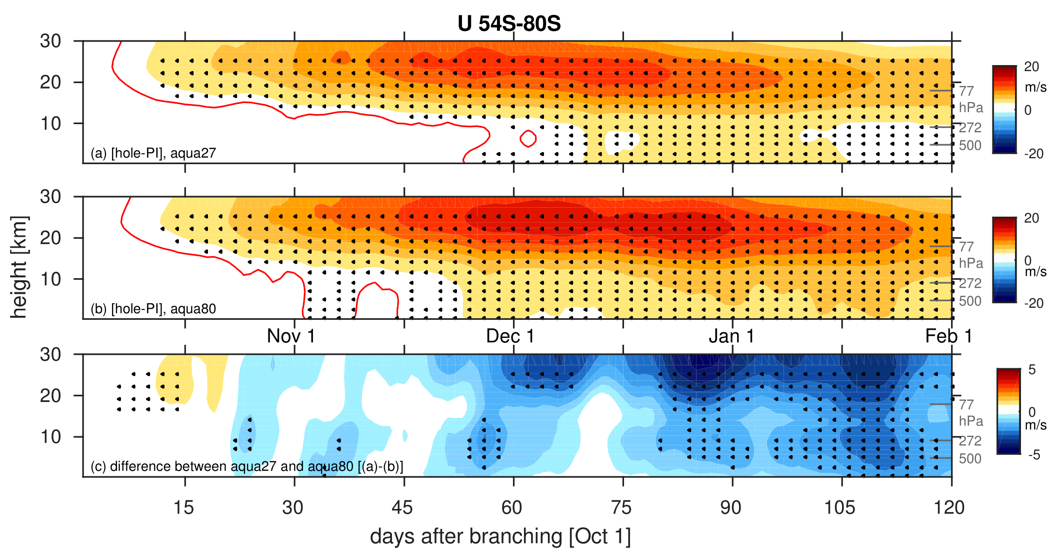

FIG. 9. Evolution of zonal wind from 54S to 80S for the [ozone hole-PI] runs for an aquaplanet (a) with “Antarctic" albedo equal to 0.27 (AQUA27), (b) with “Antarctic" albedo equal to 0.8 (AQUA80). (c) difference between (a) and (b). The 1m/s contour is indicated in red in (a) and (b).

This negative feedback caused by the presence of stationary waves can be further demonstrated by imposing the same ozone hole in the Northern Hemisphere. We compare the response of

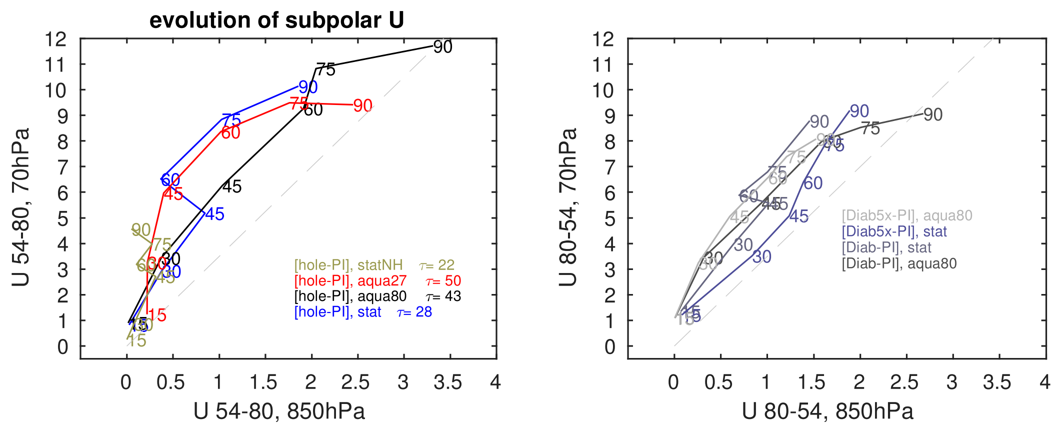

FIG. 10. Evolution of subpolar U for the (a) [ozone hole-PI] runs with (blue) realistic stationary waves, (red) an aquaplanet with “Antarctic" albedo equal to 0.27, (black) an aquaplanet with “Antarctic" albedo equal to 0.8, and (gold) Northern Hemisphere with realistic stationary waves. (b) runs analogous to [ozone hole-PI] but in which a diabatic heating perturbation is imposed directly (see methods). The mean of each fifteen day segment after branching is indicated with a dot, and is labeled by the last day included in the fifteen day segment (e.g. 30 is for days 16 to 30). For (b), for the runs with a factor of five increase in diabatic heating rate, we divide the response by a factor of five.

subpolar zonal wind in the (y-axis) lower stratosphere and (x-axis) lower troposphere in Figure 10. Consider STAT (blue line); the average wind anomaly for days 61 to 75 is 8.8m/s at 70hPa and 1.0m/s at 850hPa, whereas in the two AQUA runs the wind responses are stronger (for AQUA80 in black, 10.8m/s at 70hPa and 2.0m/s at 850hPa). The corresponding changes for the NH (in gold) are much weaker both in the lower stratosphere and troposphere despite cooling aloft (4.0m/s and 0.3m/s respectively). The net effect is that stationary waves (of which there is more activity in the NH) help damp the surface response to ozone depletion. The stationary wave effect will be further isolated in Section 5c

It is important to note that while stationary waves damp the surface response, transient planetary waves help contribute to the surface response, in agreement with Smith and Scott (2016). We demonstrate this by considering the Eulerian mean momentum budget for AQUA80 which only contains transient planetary waves. The zonal wind tendency calculated explicitly is shown in Figure 11abc, and the various terms in terms of the budget (equation 2) are shown in the rest of Figure 11. Figure 11def shows the sum of all terms on the right-hand size of equation 2, which should be equal to the zonal wind tendency in Figure 11abc. This is indeed the case, as the budget closes in nearly all regions, though some of the fine-scale details of the wind tendencies differ. The dominant terms are the eddy forcing term (Figure 11ghi) and the coriolis torque (Figure 11jkl), with the acceleration in most regions and lags provided by the eddy forcing term. The sum of the eddy forcing and coriolis terms (Figure 11mno) already resembles the total tendency in most regions/lags (Figure 11def), but crucially in the mid- and upper- stratosphere changes in gravity wave absorption act as a negative feedback in days 31 to 70 (late spring), and dominate the response in days 71 to 120 (summer). In other words, the zonal wind anomaly peaks in December before weakening in January and February because the already accelerated vortex allows for more gravity wave absorption in the mid-stratosphere. The advection term also contributes in regions with strong wind gradients (bottom, Figure 11). The net effect is that the dominant term for the subpolar zonal acceleration is the resolved eddy term in Figure 11ghi, and importantly this acceleration extends from the stratosphere to the surface.

Figure 12 decomposes the eddy forcing into its various wavenumber components. At early lags, the tropospheric response arises mostly through wave-2 and wave-3 (Figure 12def), while for days 71 to 120 synoptic wavenumbers are most important (Figure 12ghi). The wave-2 and wave-3 present in AQUA80 are transient planetary waves, and it is clear that they help set up the initial jet shift and then contribute a continued acceleration at subpolar latitudes. Wave-1 does not contribute to forcing the jet shift (Figure 12abc). These conclusions are true of the STAT runs as well (Figure 14).

The importance of both planetary and synoptic waves is also evident using the Transformed Eulerian mean budget (as in Orr et al. 2012b). The time evolution of the upper tropospheric (200-400hPa) meridional component of the Eliassen Palm flux (EP_y) is shown in Figure 3de and 6de for STAT and AQUA80; both synoptic and planetary waves are important. The timing of the increase in EP_y is similar for both synoptic and planetary waves, however, and thus it is unclear if one can be argued to help induce the other. That being said, these figures (and also Figure 12) show that at later lags, synoptic wavenumbers dominate the response. A similar relative role for planetary waves vs. synoptic waves for the tropospheric jet shift is evident for both AQUA80 and STAT (in both Figure 3de and 6de), and hence the presence of stationary waves does not appear to affect the ability of planetary waves to contribute to the jet shift. However the jet shift is weaker for STAT (due to surface shortwave and stationary wave feedbacks) and consistent with this the overall eddy forcing is weaker too (Figure 3de vs. 6de).

c. Response of STAT and AQUA80 to stratospheric diabatic heating

In addition to the ozone hole runs presented thus far, we have also performed integrations in which a diabatic heating perturbation replaces the ozone perturbation. As discussed in Section 2, the spatial structure of the diabatic heating perturbation follows the ozone perturbation, and its magnitude (-0.5K/day) mimics that due to ozone (Figure 1d-f). The benefit from these diabatic heating runs are two-fold: first, we can increase the amplitude of this diabatic heating perturbation at will and hence explore linearity of the response. (In contrast, the impact of ozone saturates as concentrations cannot be negative.) Second, the surface shortwave heating perturbation is not present, and hence the stationary waves present in STAT but absent in AQUA80 are the only factor that can lead to a difference in the surface response.

We begin with the linearity of the response. Figure 10b is similar to Figure 10a, but showing the response to a diabatic heating perturbation imposed on STAT and AQUA80. By construction, the lower stratospheric and tropospheric wind response for a -0.5K/day perturbation (the dark purple and dark gray lines) in Figure 10b resemble qualitatively their counterpart in Figure 10a. The experiments with a factor of five times stronger perturbation (-2.5K/day) are shown in Figure 10b but with the subsequent response divided by a factor of five. It is clear that the response is generally linear. (The response in AQUA80 is slightly weaker than might be expected by linearity, though the response for STAT is stronger). This result highlights the fact that interannual variability in ozone concentrations should be useful for seasonal predictability of surface climate (Son et al. 2013; Bandoro et al. 2014; Hendon et al. 2020; Jucker and Goyal 2021).

Next, we use these diabatic forcing experiments to isolate the role of stationary waves for the downward response, as these experiments do not allow for the shortwave surface feedback mechanism from Section 5a. The subpolar zonal wind response for STAT and AQUA80 to an identical perturbation is shown in Figure 13a and 13b, and the difference between the two is in Figure 13c. Initially, the diabatic perturbation causes a larger response in STAT, but the zonal wind response in AQUA80 in both the stratosphere and troposphere becomes larger after day 45. Hence, stationary waves lead to a negative feedback on the response even if surface shortwave feedbacks

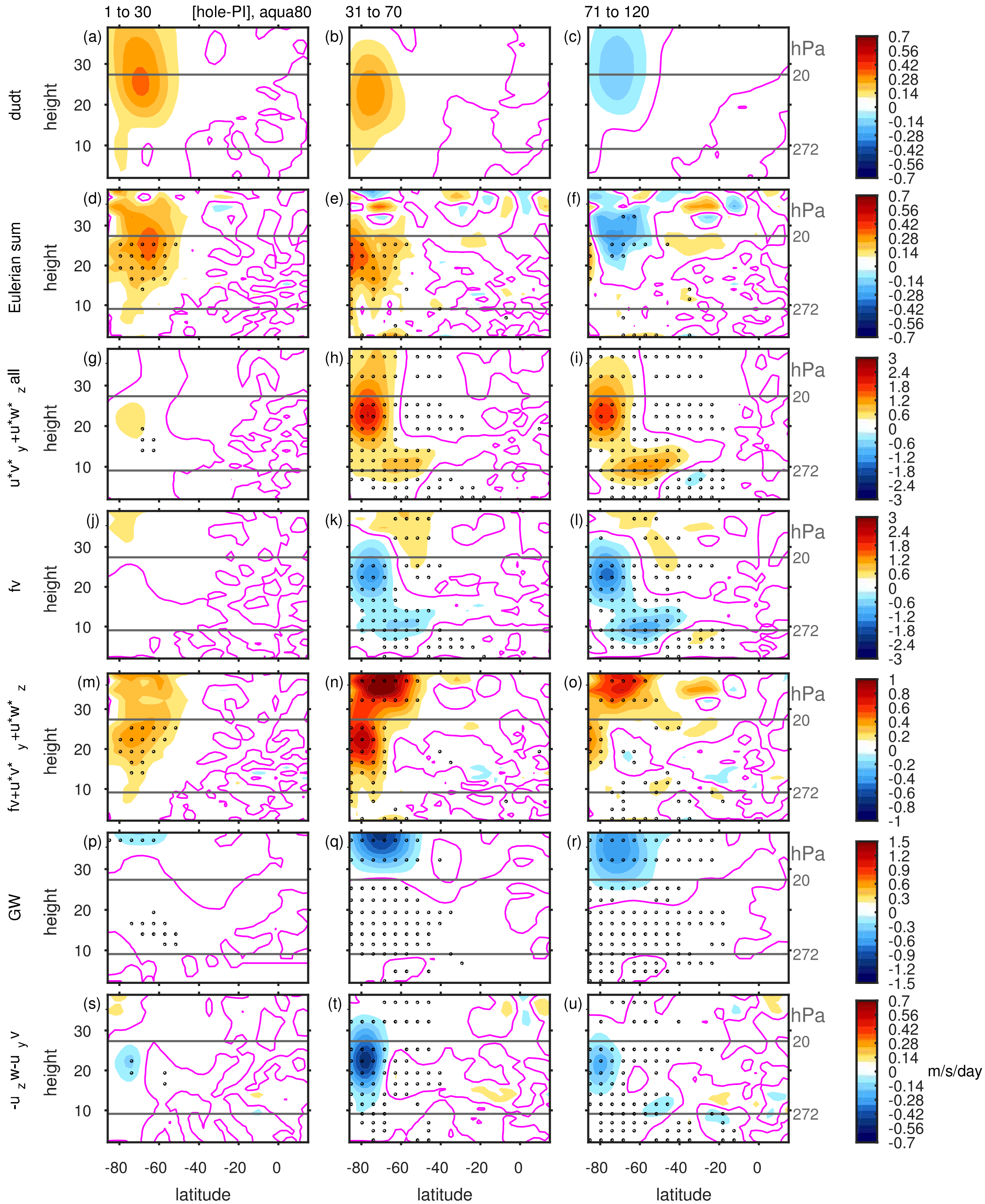

FIG. 11. Eulerian mean momentum budget for the [ozone hole-PI] aquaplanet runs, with “Antarctic" albedo equal to 0.8 in (left) days 1-30 after branching, i.e. October; (middle) days 31 to 70; (right) days 71 to 120. (a-c) total wind tendency; (d-f) sum of all terms; (g-i) eddy forcing terms (u’v’ and u’w’); (j-l) coriolis torque; (m-o) sum of eddy forcing and coriolis torque; (p-r) gravity wave drag; (s-u) advection of mean zonal wind. Note that the color-bar for (g-i) and (j-l) differ from that in (m-o) due to the strong cancellation between eddy forcing and coriolis torque (as expected).

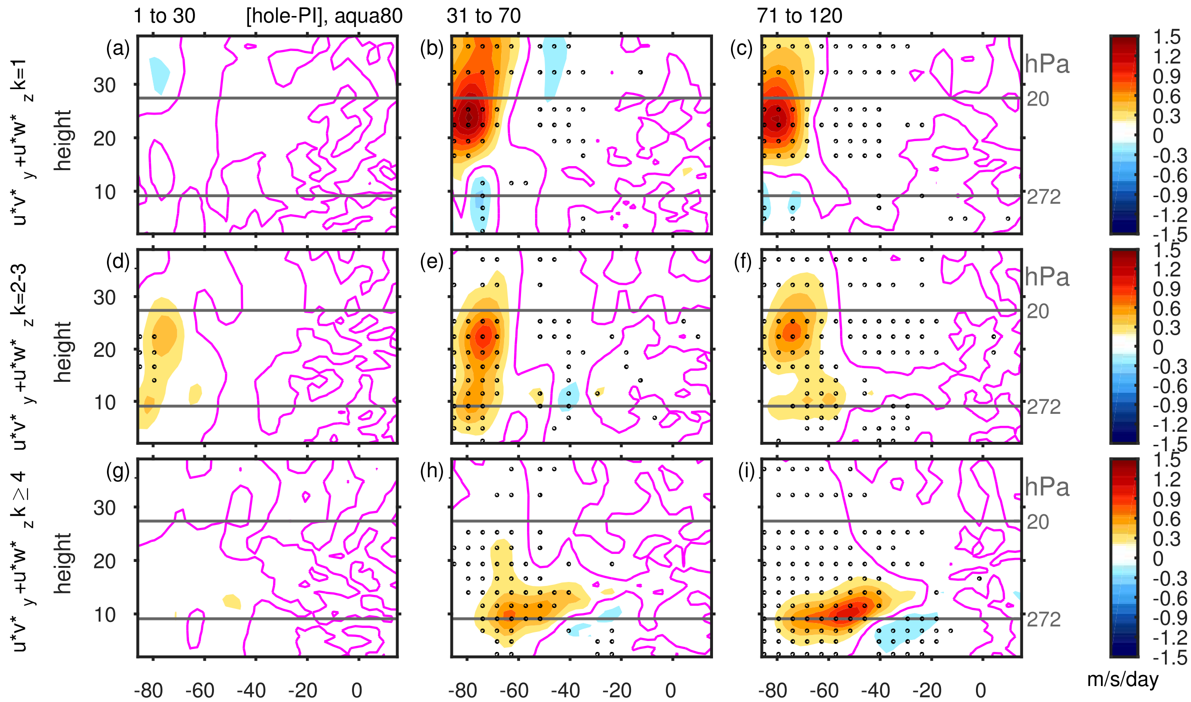

FIG. 12. Decomposition of the eddy forcing term in 11ghi into the various wavenumber components. (a-c) wavenumber 1; (d-f) wavenumber 2 through 3; (g-i) wavenumbers 4 and larger.

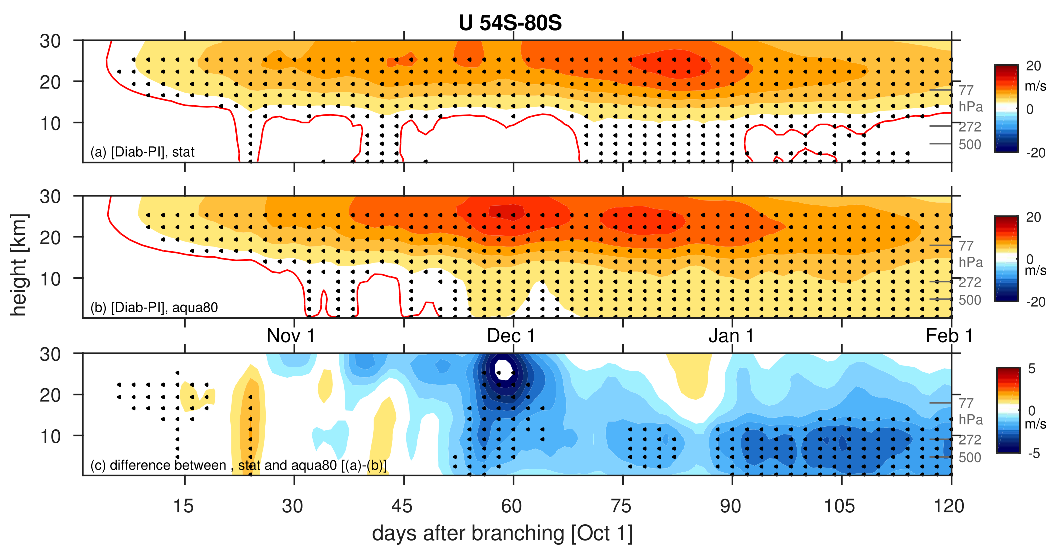

FIG. 13. Evolution of zonal wind from 54S to 80S for the Diabatic-PI runs with (a) realistic stationary waves, (b) an aquaplanet, with “Antarctic" albedo equal to 0.8. (c) difference between (a) and (b). The 1m/s contour is indicated in red in (a) and (b).

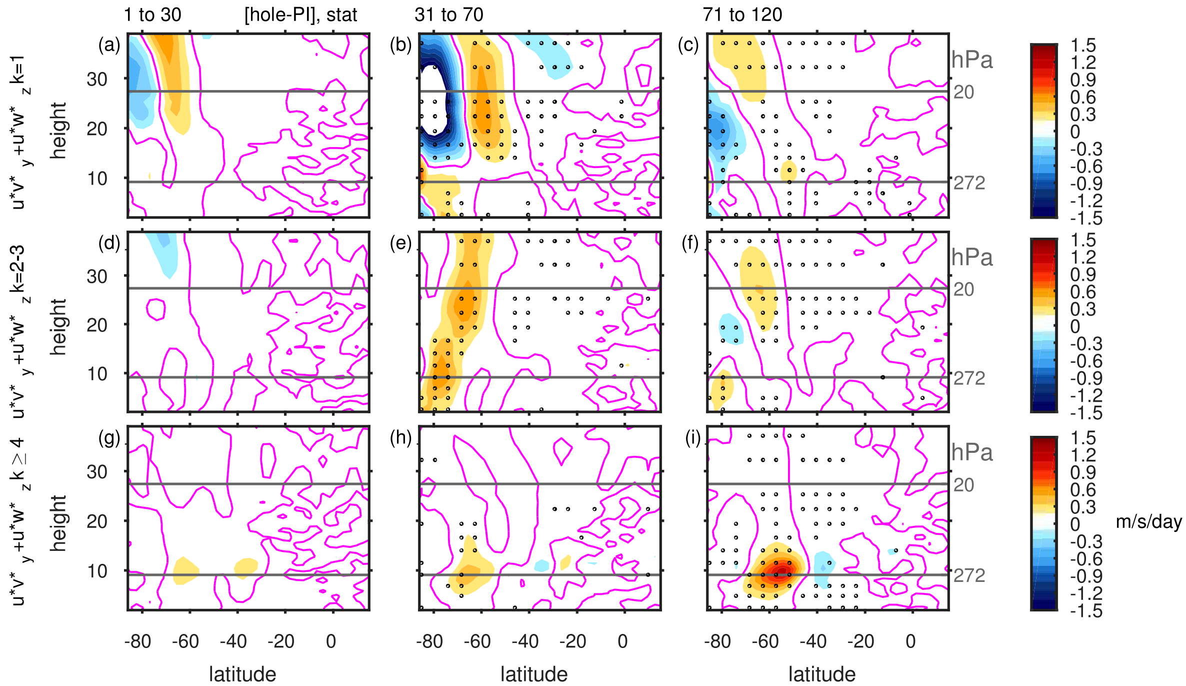

FIG. 14. As in 12 but for STAT.

are suppressed, but this stationary wave feedback develops slowly. We speculate that the stationary wave effect is connected to the delayed breakup of the vortex; it manifests itself only late in the season when the vortex is already gone in the PI control simulation.

d. Relative roles of stationary waves and shortwave feebacks

We have demonstrated that there are two distinct effects that lead to a weaker response to ozone depletion in STAT as compared to AQUA80: surface shortwave feedbacks and stationary waves that partially compensate the cooling of the pole due to ozone loss. The two effects were isolated in Figure 9 (for shortwave feedbacks) and Figure 13 (for stationary wave feedbacks). This delineation of the two effects allows us to ask the question: Which of the two is more important?

A comparison of Figure 9c and Figure 13c indicates that the shortwave effect is quicker to begin, and is already present by day 20. Its amplitude subsequently increases over time as the summer solstice is approached. In contrast, the stationary wave effect does not manifest itself until late in the season when the vortex is already strengthened, and thus the difference in Figure 13c is only significant after day 50 (late November). After the effect begins however, it is stronger than the shortwave effect and persists with roughly similar magnitude through the rest of summer. The net effect is that the shortwave effect is most important in November, the stationary wave effect is most important in December, and both are of roughly equal importance in January.

6. Discussion and Conclusions

Ozone depletion is known to have been the dominant contributor to a poleward shift of the Southern Hemisphere (SH) tropospheric midlatitude jet, precipitation, and storm tracks over the late 20th century. Over the next 50 years, ozone recovery is expected to nearly cancel out changes in the jet and Hadley Cell that would otherwise be forced by greenhouse gases (Polvani et al. 2011; Arblaster et al. 2011; Barnes and Polvani 2013; Gerber and Son 2014; Waugh et al. 2015; Seviour et al. 2017; Son et al. 2018; Banerjee et al. 2020). The degree of cancellation is uncertain and model dependent, however, leading to uncertainty in future projections (Gerber and Son 2014). The mechanism whereby ozone depletion leads to a downward impact, and the details of how this mechanism governs the magnitude of the impact, are still unclear (as noted in WMO Ozone assessments in 2010, 2014, and 2018). While previous work has shown that jet latitude (Garfinkel et al. 2013b) and the details of the ozone forcing (Neely et al. 2014; Young et al. 2014) are important, we have demonstrated two additional processes that are important for the downward impact: surface shortwave effects and stationary waves.

This study takes advantage of a recently developed intermediate complexity model that can delineate the role of these two effects. First, we integrate it with realistic stationary waves, comparing it to runs without any zonal asymmetry in the bottom boundary. Second, we compared integrations with an ozone hole in which surface shortwave feedbacks are present, to integrations with a diabatic temperature tendency that mimics the shortwave effects of ozone depletion in the stratosphere only. This flexibility allowed us to isolate the role of stationary waves and surface shortwave changes for the surface response.

In the most realistic configuration (STAT), the model simulates a response resembling that observed and simulated by comprehensive models (Figure 1, 2, and 3). When an identical ozone hole is imposed in an aquaplanet configuration (AQUA80), the response is twice as strong for many of the diagnostics examined (Figure 1mno, 5, and 6). The realistic and aquaplanet configurations differ in at least two aspects potentially relevant to the ozone hole response: stationary waves and surface shortwave effects.

The importance of surface shortwave effects was isolated by comparing an aquaplanet configuration with an albedo of 0.8 over Antarctica (AQUA80) to a similar configuration but with an albedo of 0.27 (AQUA27; Figure 9), as the stationary waves are identical in these configurations. The poleward jet shift is significantly stronger in AQUA80 than in AQUA27 by late October, and in January the tropospheric response is more than a factor of two stronger in AQUA80. The stratospheric response is also stronger in AQUA80 because the colder lower tropospheric column also impacts geopotential height in the stratosphere, as can be diagnosed using the hypsometric equation.

The importance of stationary waves was isolated by comparing the response to a stratospheric diabatic heating perturbation of similar strength and spatial structure to that caused by ozone depletion in both AQUA80 and STAT (Figure 13ab). The only factor that can explain a difference in response (Figure 13c) is a stationary wave feedback, as surface shortwave effects are not present. The presence of stationary waves leads to a weaker response starting in late November and extending into February to an identical diabatic heating perturbation. This effect arises because a stationary wave negative feedback leads to a weaker stratospheric circulation response when there are stationary waves in the troposphere.

Despite the negative stationary wave feedback on the magnitude of the stratospheric circulation response to ozone depletion, tropospheric planetary waves are important for the tropospheric jet response. Both planetary and synoptic waves are important for the tropospheric jet shift both in AQUA80 and STAT integrations (Figures 12 and 14). Waves 1-3 contribute roughly half of the torque in November, though by December and January their contribution is less (Figure 3de and 6de). This is true for both of the ozone depletion runs, and also the diabatic heating runs where we can increase the amplitude of the forcing to better capture the response (Figure 15).

Gravity waves also act as a negative feedback on the magnitude of the stratospheric circulation response to ozone depletion. Namely, the strengthened polar vortex allows more gravity waves to propagate into the stratosphere, and these gravity waves then break in the subpolar mid-stratosphere (Figure 11). This partial compensation between gravity waves and an externally imposed forcing is consistent with Cohen et al. (2013); Sigmond and Shepherd (2014); Scheffler and Pulido (2015); Watson and Gray (2015), and Garfinkel and Oman (2018).

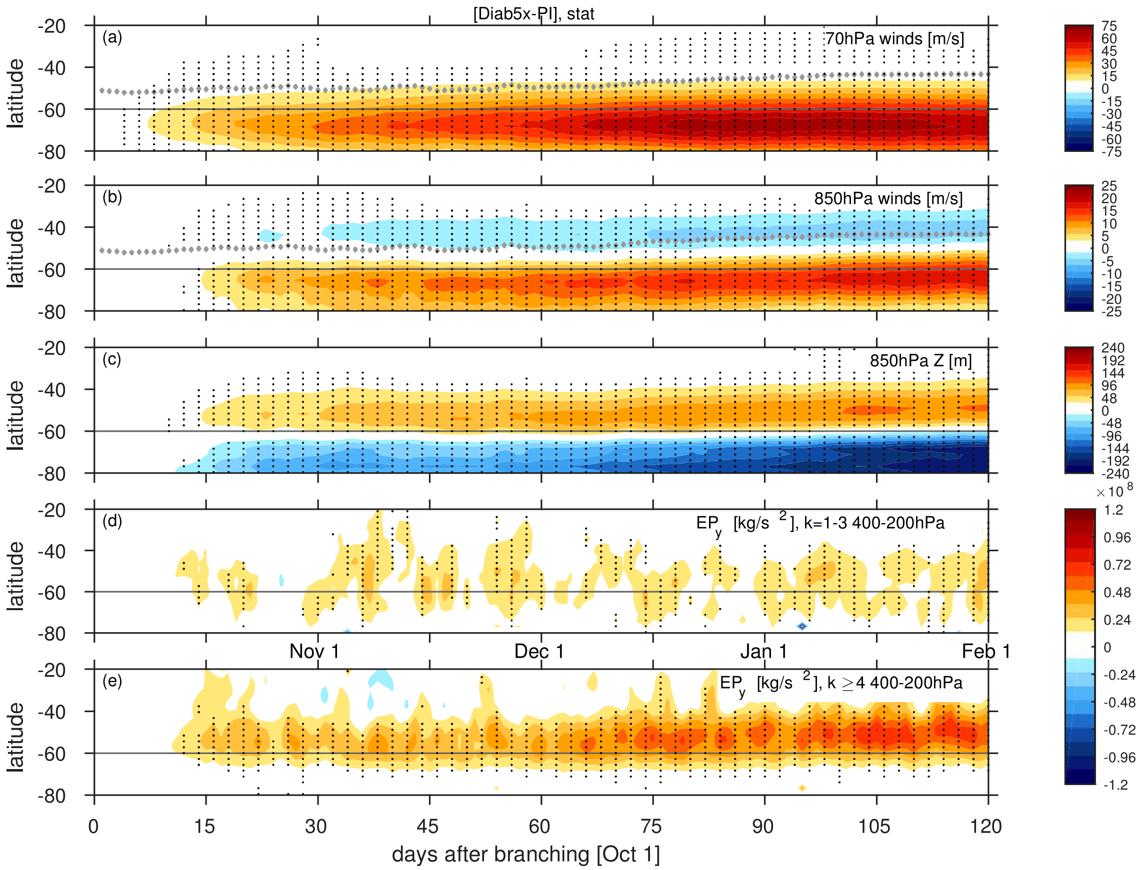

FIG. 15. As in Figure 3 but for a diabatic heating rate of 2.5K/day in the lower stratosphere and no ozone depletion. Note factor of 5 difference in colorbar for (a) and (b), and factor of 2 difference for (c)-(e).

The response in AQUA27 is weaker than in AQUA80 despite the fact that the jet is further equatorward and the annular mode timescale larger in AQUA27, two factors that would lead to a stronger response (Garfinkel et al. 2013b). This indicates that the surface shortwave effect in AQUA27 overwhelms the jet latitude/eddy feedback strength effect. In order to cleanly assess the eddy feedback strength effect highlighted by Garfinkel et al. (2013b), we have performed an experiment using the AQUA80 configuration but in which the jet is pushed 7° further poleward. This is achieved by imposing a stronger and more poleward meridional ocean heat transport gradient following equation A8 of Garfinkel et al. (2020a) with an amplitude of $50Wm^{-2}$, which leads to a poleward shift of the sea surface temperature gradient. The response to ozone depletion is shown in supplemental Figure 1, and it is clear that the tropospheric response is weaker as expected. The stationary waves and surface shortwave effects are identical in this simulation to those in AQUA80, and hence the weakened tropospheric response is due to jet latitude and weakened eddy feedback. Note that this run includes a stronger sea surface temperature front than AQUA80 yet has a weaker response, suggesting that the results of Ogawa et al. (2015) may have more to do with the eddy feedback strength in their simulations than the well-defined sea surface temperature front per se.

The specific mechanism as to how the downward influence arises is not the main focus of this paper, however our results are of relevance to previously proposed theories. Wave-2 and wave-3 are crucial in the lower stratospheric zonal momentum response (Figures 12 and 14, consistent with Orr et al. 2012b). Both planetary and synoptic waves are important for the tropospheric impact, and it is impossible to distinguish whether one begins before the other. This difficulty occurs even if we enhance the signal-to-noise ratio by imposing a diabatic heating perturbation five times stronger than that associated with ozone depletion (Figure 15de), likely because of eddy-eddy interactions (Domeisen et al. 2013; Smith and Scott 2016). Synoptic waves are somewhat more important in summer, but in late fall the momentum forcing is more evenly split between synoptic and planetary waves. This balance is evident both in AQUA80 and in STAT.

In all runs, a tropospheric response does not begin until at least day 15, and in the diabatic heating runs with the forcing increased by a factor of five, there is even a weak equatorward shift in the first ten days (though not evident in Figure 15b using the chosen contour interval). This arises because a thermally driven cooling of the vortex will be balanced in part by downwelling over the pole and equatorward motion in the troposphere, which leads to an easterly Coriolis torque (Eliassen 1951). This opposite response is consistent with Yang et al. (2015) who also find that the residual circulation is of the wrong sign to explain the poleward shift, and also with White et al. (2020) who also impose a diabatic heating perturbation and find that the poleward shift does not occur for at least 15 days. This effect does not explain why the observed poleward shift is not robust until December, however, as this delay is far longer than 15 days.

On the other hand, our simulations help clarify the important factors for the onset of the response. Namely, the tropospheric response can begin in late October if the forcing is strong (Figure 15b) or in AQUA80 (Figure 6b). The tropospheric response begins first at subpolar latitudes and only later, after synoptic eddies dominate, includes the midlatitudes. The net effect is that the delay until December in STAT is a consequence of the two negative feedbacks - stationary waves and surface shortwave effects - that both weaken and postpone the response until after the ozone hole is already filling up. Future work should evaluate whether these negative feedbacks are crucial for the timing of the onset of the response in observations as well.

The response to an identical ozone hole imposed in the Northern Hemisphere in STAT (STATNH) is significantly weaker than when imposed in the Southern Hemisphere (Supplemental Figure 2). In other words, the tropospheric circulation in the Northern Hemisphere is less sensitive to a stratospheric ozone perturbation. Both of the negative feedbacks we identified - stationary waves and surface shortwave effects - likely play a role. Northern Hemisphere stationary waves are stronger, and hence the stratospheric circulation response to an identical ozone depletion is weaker due to an offset by enhanced wave propagation into the stratosphere. Second, the Arctic includes more regions with lower albedo as compared to the Antarctic. In addition, the annular mode timescale is shorter in the Northern Hemisphere (22 days; Figure 10), and hence synoptic eddy feedbacks are weaker too.

While the model used in this work suffers from some limitations - there is no coupling of the ozone with the dynamics, the imposed ozone hole has no zonal structure, and the albedo is constant for all shortwave wavelengths - the results of our work have implications for seasonal forecasting and for the interpretation of results from both comprehensive and idealized models. First, interannual variability in ozone concentrations can be used to enhance seasonal forecasting (Figure 10), consistent with Hendon et al. (2020) and Jucker and Goyal (2021). Second, dry and flat idealized models miss both the stationary wave and shortwave effects, and the lack of these effects can lead to an exaggerated doubling of the response to an identical ozone hole. Third, the surface radiative budget over the Antarctic surface and boundary layer is crucial for getting the correct temperature response to ozone depletion for the right reasons, and it is not clear how well models can capture the stable boundary layers common over Antarctica, the mixed-phase and ice clouds common at these latitudes, or the properties of a glaciated land surface. Future work should explore whether diversity in how models represent these processes can explain some of the diversity in future projections of climate change in the Southern Hemisphere (Gerber and Son 2014), and thereby help narrow projections as ozone recovers.

Acknowledgments. CIG and IW acknowledge the support of a European Research Council starting grant under the European Union Horizon 2020 research and innovation programme (grant agreement number 677756). EPG acknowledges support from the US NSF through grant AGS 1852727.

MJ acknowledges support from the Australian Research Council (ARC) Centre of Excellence for Climate Extremes (CE170100023) and ARC grant FL 150100035. SWS was supported by the National Research Foundation of Korea (NRF) grant funded by the Korea government (Ministry of Science and ICT 2017R1E1A1A01074889.

Data availability statement. The updated version of MiMA used in this study including the modified source code can be downloaded from https://github.com/ianpwhite/MiMA/releases/tag/MiMA-ThermalForcing-v1.0beta (with DOI: https://doi.org/10.5281/zenodo.4523199).

References

Andrews, D. G., J. R. Holton, and C. B. Leovy, 1987: *Middle Atmosphere Dynamics*. Academic Press.

Arblaster, J. M., G. A. Meehl, and D. J. Karoly, 2011: Future climate change in the southern hemisphere: Competing effects of ozone and greenhouse gases. *Geophysical Research Letters*, **38 (2)**.

Baldwin, M. P., D. B. Stephenson, D. W. J. Thompson, T. J. Dunkerton, A. J. Charlton, and A. O'Neill, 2003: Stratospheric memory and skill of extended-range weather forecasts. *Science*, **301**, doi:10.1126/science.1087143.

Bandoro, J., S. Solomon, A. Donohoe, D. W. Thompson, and B. D. Santer, 2014: Influences of the antarctic ozone hole on southern hemispheric summer climate change. *Journal of Climate*, **27 (16)**, 6245–6264.

Banerjee, A., J. C. Fyfe, L. M. Polvani, D. Waugh, and K.-L. Chang, 2020: A pause in southern hemisphere circulation trends due to the montreal protocol. *Nature*, **579 (7800)**, 544–548.

Barnes, E. A., and L. Polvani, 2013: Response of the midlatitude jets, and of their variability, to increased greenhouse gases in the cmip5 models. *Journal of Climate*, **26 (18)**, 7117–7135, doi:10.1175/JCLI-D-12-00536.1.

Betts, A., and M. Miller, 1986: A new convective adjustment scheme. part ii: Single column tests using gate wave, bomex, atex and arctic air-mass data sets. *Quarterly Journal of the Royal Meteorological Society*, **112 (473)**, 693–709, doi:10.1002/qj.49711247308.

Betts, A. K., 1986: A new convective adjustment scheme. part i: Observational and theoretical basis. *Quarterly Journal of the Royal Meteorological Society*, **112 (473)**, 677–691, doi:10.1002/qj.49711247307.

Checa-Garcia, R., 2018: Cmip6 ozone forcing dataset: supporting information. *Zenodo*, URL https://doi.org/10.5281/zenodo.1135127.

Checa-Garcia, R., M. I. Hegglin, D. Kinnison, D. A. Plummer, and K. P. Shine, 2018: Historical tropospheric and stratospheric ozone radiative forcing using the cmip6 database. *Geophysical Research Letters*, **45 (7)**, 3264–3273.

Chiodo, G., L. Polvani, and M. Previdi, 2017: Large increase in incident shortwave radiation due to the ozone hole offset by high climatological albedo over antarctica. *Journal of Climate*, **30 (13)**, 4883–4890.

Cohen, N. Y., E. P. Gerber, and E. P. Oliver Bühler, 2013: Compensation between resolved and unresolved wave driving in the stratosphere: Implications for downward control. *Journal of the Atmospheric Sciences*, **70 (12)**, 3780–3798, doi:10.1175/JAS-D-12-0346.1.

Domeisen, D. I., L. Sun, and G. Chen, 2013: The role of synoptic eddies in the tropospheric response to stratospheric variability. *Geophysical research letters*, **40 (18)**, 4933–4937.

Eliassen, A., 1951: Slow thermally or frictionally controlled meridional circulation in a circular vortex. *Astrophysica Norvegica*, **5**, 19.

Eyring, V., and Coauthors, 2013: Long-term ozone changes and associated climate impacts in cmip5 simulations. *Journal of Geophysical Research: Atmospheres*, **118 (10)**, 5029–5060, doi:10.1002/jgrd.50316.

Frierson, D. M., I. M. Held, and P. Zurita-Gotor, 2006: A gray-radiation aquaplanet moist gcm. part i: Static stability and eddy scale. *Journal of the atmospheric sciences*, **63 (10)**, 2548–2566, doi:10.1175/JAS3753.1.

Frierson, D. M., I. M. Held, and P. Zurita-Gotor, 2007: A gray-radiation aquaplanet moist gcm. part ii: Energy transports in altered climates. *Journal of the atmospheric sciences*, **64 (5)**, 1680–1693, doi:10.1175/JAS3913.1.

Garcia, R. R., D. E. Kinnison, and D. R. Marsh, 2012: "world avoided" simulations with the whole atmosphere community climate model. *Journal of Geophysical Research: Atmospheres*, **117 (D23)**.

Gardner, A. S., and M. J. Sharp, 2010: A review of snow and ice albedo and the development of a new physically based broadband albedo parameterization. *Journal of Geophysical Research: Earth Surface*, **115 (F1)**.

Garfinkel, C., and L. Oman, 2018: Effect of gravity waves from small islands in the southern ocean on the southern hemisphere atmospheric circulation. *Journal of Geophysical Research: Atmospheres*, **123 (3)**, 1552–1561.

Garfinkel, C., D. W. Waugh, and E. Gerber, 2013a: Effect of tropospheric jet latitude on coupling between the stratospheric polar vortex and the troposphere. *J. Clim.*, **26 (6)**, 2077–2095, doi:10.1175/JCLI-D-12-00301.1.

Garfinkel, C. I., D. W. Waugh, and E. P. Gerber, 2013b: The effect of tropospheric jet latitude on coupling between the stratospheric polar vortex and the troposphere. *Journal of Climate*, **26 (6)**, doi:10.1175/JCLI-D-12-00301.1.

Garfinkel, C. I., I. White, E. P. Gerber, and M. Jucker, 2020a: The impact of sst biases in the tropical east pacific and agulhas current region on atmospheric stationary waves in the southern hemisphere. *Journal of Climate*, **33 (21)**, 9351–9374.

Garfinkel, C. I., I. P. White, E. P. Gerber, and M. Jucker, 2020b: The building blocks of northern hemisphere wintertime stationary waves. *Journal of Climate*, **33 (13)**, doi:10.1175/JCLI-D-19-0181.1.

Gerber, E. P., and L. M. Polvani, 2009: Stratosphere-troposphere coupling in a relatively simple agcm: The importance of stratospheric variability. *J. Clim.*, **22**, 1920–1933, doi:10.1175/2008JCLI2548.1.

Gerber, E. P., L. M. Polvani, and D. Ancukiewicz, 2008: Annular mode time scales in the Intergovernmental Panel on Climate Change Fourth Assessment Report models. *Geophys. Res. Lett.*, **35**, L22707, doi:10.1029/2008GL035712.

Gerber, E. P., and S.-W. Son, 2014: Quantifying the summertime response of the austral jet stream and hadley cell to stratospheric ozone and greenhouse gases. *Journal of Climate*, **27**, doi:10.1175/JCLI-D-13-00539.1.

Gillett, N. P., and D. W. Thompson, 2003: Simulation of recent southern hemisphere climate change. *Science*, **302 (5643)**, 273–275.

Gonzalez, P. L., L. M. Polvani, R. Seager, and G. J. Correa, 2014: Stratospheric ozone depletion: a key driver of recent precipitation trends in south eastern south america. *Climate Dynamics*, **42 (7-8)**, 1775–1792.

Grenfell, T. C., S. G. Warren, and P. C. Mullen, 1994: Reflection of solar radiation by the antarctic snow surface at ultraviolet, visible, and near-infrared wavelengths. *Journal of Geophysical Research: Atmospheres*, **99 (D9)**, 18 669–18 684.

Grise, K. M., D. W. Thompson, and P. M. Forster, 2009: On the role of radiative processes in stratosphere–troposphere coupling. *Journal of climate*, **22 (15)**, 4154–4161.

Hendon, H., E.-P. Lim, and S. Abhik, 2020: Impact of interannual ozone variations on the downward coupling of the 2002 southern hemisphere stratospheric warming. *Journal of Geophysical Research: Atmospheres*, **125 (16)**, e2020JD032 952.

Hendon, H. H., D. W. Thompson, and M. C. Wheeler, 2007: Australian rainfall and surface temperature variations associated with the southern hemisphere annular mode. *Journal of Climate*, **20 (11)**, 2452–2467.

Hitchcock, P., and I. R. Simpson, 2016: Quantifying eddy feedbacks and forcings in the tropospheric response to stratospheric sudden warmings. *Journal of the Atmospheric Sciences*, **73 (9)**, 3641–3657.

Hurwitz, M. M., P. A. Newman, and C. I. Garfinkel, 2011: The Arctic vortex in March 2011: a dynamical perspective. *Atm. Chem. Phys.*, **11**, 11 447–11 453, doi:10.5194/acp-11-11447-2011.

Hurwitz, M. M., P. A. Newman, F. Li, L. D. Oman, O. Morgenstern, P. Braesicke, and J. A. Pyle, 2010: Assessment of the breakup of the Antarctic polar vortex in two new chemistry-climate models. *Journal of Geophysical Research (Atmospheres)*, **115**, D07 105, doi:10.1029/2009JD012788.

Iacono, M. J., E. J. Mlawer, S. A. Clough, and J.-J. Morcrette, 2000: Impact of an improved longwave radiation model, rrtm, on the energy budget and thermodynamic properties of the ncar community climate model, ccm3. *Journal of Geophysical Research: Atmospheres*, **105 (D11)**, 14 873–14 890.

Jucker, M., and E. Gerber, 2017: Untangling the annual cycle of the tropical tropopause layer with an idealized moist model. *Journal of Climate*, **30 (18)**, 7339–7358.

Jucker, M., and R. Goyal, 2021: Ozone-forced southern annular mode during antarctic stratospheric warming events. *Earth and Space Science Open Archive ESSOAr*.

Kållberg, P., P. Berrisford, B. Hoskins, A. Simmons, S. Lamy-thépaut, and R. Hine, 2005: *ERA-40 atlas*. ERA-40 Project Report Series 19, ECMWF, 103 pp.

Kang, S. M., L. M. Polvani, J. C. Fyfe, and M. Sigmond, 2011: Impact of Polar Ozone Depletion on Subtropical Precipitation. *Science*, **332**, 951–, doi:10.1126/science.1202131.

Karpechko, A. Y., A. L. A. Maycock, M. Abalos, H. Akiyoshi, J. Arblaster, C. Garfinkel, K. Rosenlof, and M. Sigmond, 2018: *Stratospheric Ozone Changes and Climate, Chapter 5 in Scientific Assessment of Ozone Depletion*. Global Ozone Research and Monitoring Project Rep. No. 58, 416 pp.

Kidson, J. W., 1988: Interannual variations in the southern hemisphere circulation. *Journal of Climate*, **1 (12)**, 1177–1198.

Kushner, P. J., and L. M. Polvani, 2004: Stratosphere-troposphere coupling in a relatively simple agcm: The role of eddies. *J. Clim.*, **17**, 629–639.

Lawrence, Z. D., J. Perlwitz, A. H. Butler, G. L. Manney, P. A. Newman, S. H. Lee, and E. R. Nash, 2020: The remarkably strong arctic stratospheric polar vortex of winter 2020: Links to record-breaking arctic oscillation and ozone loss. *Journal of Geophysical Research: Atmospheres*, **125 (22)**, e2020JD033 271.

Li, F., P. A. Newman, and R. S. Stolarski, 2010: Relationships between the brewer-dobson circulation and the southern annular mode during austral summer in coupled chemistry-climate model simulations. *Journal of Geophysical Research: Atmospheres*, **115 (D15)**.

Manney, G. L., and Coauthors, 2011: Unprecedented arctic ozone loss in 2011. *Nature*, **478 (7370)**, 469–475.

Manzini, E., B. Steil, C. Brühl, M. A. Giorgetta, and K. Krüger, 2003: A new interactive chemistry-climate model: 2. sensitivity of the middle atmosphere to ozone depletion and increase in greenhouse gases and implications for recent stratospheric cooling. *Journal of Geophysical Research: Atmospheres*, **108 (D14)**.

McLandress, C., A. I. Jonsson, D. A. Plummer, M. C. Reader, J. F. Scinocca, and T. G. Shepherd, 2010: Separating the dynamical effects of climate change and ozone depletion. part i: Southern hemisphere stratosphere. *Journal of Climate*, **23 (18)**, 5002–5020, doi:10.1175/2010JCLI3586.1.

McLandress, C., T. G. Shepherd, J. F. Scinocca, D. A. Plummer, M. Sigmond, A. I. Jonsson, and M. C. Reader, 2011: Separating the dynamical effects of climate change and ozone depletion. part ii: Southern hemisphere troposphere. *Journal of Climate*, **24 (6)**, 1850–1868.

Merlis, T. M., T. Schneider, S. Bordoni, and I. Eisenman, 2013: Hadley circulation response to orbital precession. part ii: Subtropical continent. *Journal of Climate*, **26 (3)**, 754–771.

Mlawer, E. J., S. J. Taubman, P. D. Brown, M. J. Iacono, and S. A. Clough, 1997: Radiative transfer for inhomogeneous atmospheres: Rrtm, a validated correlated-k model for the longwave. *Journal of Geophysical Research: Atmospheres*, **102 (D14)**, 16 663–16 682.

Neely, R., D. Marsh, K. Smith, S. Davis, and L. Polvani, 2014: Biases in southern hemisphere climate trends induced by coarsely specifying the temporal resolution of stratospheric ozone. *Geophysical Research Letters*, **41 (23)**, 8602–8610, doi:10.1002/2014GL061627.

Newman, P., and Coauthors, 2009: What would have happened to the ozone layer if chlorofluorocarbons (cfcs) had not been regulated? *Atmospheric Chemistry and Physics*, **9 (6)**, 2113–2128.

Ogawa, F., N.-E. Omrani, K. Nishii, H. Nakamura, and N. Keenlyside, 2015: Ozone-induced climate change propped up by the southern hemisphere oceanic front. *Geophysical Research Letters*, **42 (22)**, 10–056.

Orr, A., T. J. Bracegirdle, J. S. Hosking, W. Feng, H. K. Roscoe, and J. D. Haigh, 2012a: Strong dynamical modulation of the cooling of the polar stratosphere associated with the antarctic ozone hole. *Journal of Climate*, **26 (2)**, 662–668.

Orr, A., T. J. Bracegirdle, J. S. Hosking, T. Jung, J. D. Haigh, T. Phillips, and W. Feng, 2012b: Possible dynamical mechanisms for southern hemisphere climate change due to the ozone hole. *Journal of the Atmospheric Sciences*, **69 (10)**, 2917–2932.

Polvani, L. M., M. Previdi, and C. Deser, 2011: Large cancellation, due to ozone recovery, of future southern hemisphere atmospheric circulation trends. *Geophysical Research Letters*, **38 (4)**, doi:DOI:10.1029/2011GL046712.

Polvani, L. M., D. W. Waugh, G. J. P. Correa, and S.-W. Son, 2011: Stratospheric Ozone Depletion: The Main Driver of Twentieth-Century Atmospheric Circulation Changes in the Southern Hemisphere. *Journal of Climate*, **24**, 795–812, doi:10.1175/2010JCLI3772.1.

Previdi, M., and L. M. Polvani, 2014: Climate system response to stratospheric ozone depletion and recovery. *Quarterly Journal of the Royal Meteorological Society*, **140 (685)**, 2401–2419, doi: https://doi.org/10.1002/qj.2330, URL https://rmets.onlinelibrary.wiley.com/doi/abs/10.1002/qj.2330, https://rmets.onlinelibrary.wiley.com/doi/pdf/10.1002/qj.2330.

Randel, W. J., and Coauthors, 2009: An update of observed stratospheric temperature trends. *Journal of Geophysical Research: Atmospheres*, **114 (D2)**, doi:10.1029/2008JD010421, URL http://dx.doi.org/10.1029/2008JD010421.

Rao, J., and C. I. Garfinkel, 2020: Arctic ozone loss in march 2020 and its seasonal prediction in cfsv2: A comparative study with the 1997 and 2011 cases. *Journal of Geophysical Research: Atmospheres*, **125 (21)**, e2020JD033 524.

Rao, J., and C. I. Garfinkel, 2021: The strong stratospheric polar vortex in march 2020 in sub-seasonal to seasonal models: Implications for empirical prediction of the low arctic total ozone extreme. *Journal of Geophysical Research: Atmospheres*, **126 (9)**, e2020JD034 190.

Scheffler, G., and M. Pulido, 2015: Compensation between resolved and unresolved wave drag in the stratospheric final warmings of the southern hemisphere. *Journal of the Atmospheric Sciences*, **72 (11)**, 4393–4411, doi:10.1175/JAS-D-14-0270.1.

Seviour, W. J., D. W. Waugh, L. M. Polvani, G. J. Correa, and C. I. Garfinkel, 2017: Robustness of the simulated tropospheric response to ozone depletion. *Journal of Climate*, **30 (7)**, 2577–2585.

Sheshadri, A., and R. A. Plumb, 2016: Sensitivity of the surface responses of an idealized agcm to the timing of imposed ozone depletion-like polar stratospheric cooling. *Geophysical Research Letters*, **43 (5)**, 2330–2336, doi:https://doi.org/10.1002/2016GL067964, URL https://agupubs.onlinelibrary.wiley.com/doi/abs/10.1002/2016GL067964, https://agupubs.onlinelibrary.wiley.com/doi/pdf/10.1002/2016GL067964.

Sigmond, M., and T. G. Shepherd, 2014: Compensation between resolved wave driving and parameterized orographic gravity wave driving of the brewer–dobson circulation and its response to climate change. *Journal of Climate*, **27 (14)**, 5601–5610, doi:10.1175/JCLI-D-13-00644.1.

Smith, K. L., and R. K. Scott, 2016: The role of planetary waves in the tropospheric jet response to stratospheric cooling. *Geophysical Research Letters*, **43 (6)**, 2904–2911, doi:https://doi.org/10.1002/2016GL067849, URL https://agupubs.onlinelibrary.wiley.com/doi/abs/10.1002/2016GL067849, https://agupubs.onlinelibrary.wiley.com/doi/pdf/10.1002/2016GL067849.

Solomon, S., R. R. Garcia, F. S. Rowland, and D. J. Wuebbles, 1986: On the depletion of Antarctic ozone. *nature*, **321**, 755–758, doi:10.1038/321755a0.

Solomon, S., R. W. Portmann, T. Sasaki, D. J. Hofmann, and D. W. Thompson, 2005: Four decades of ozonesonde measurements over antarctica. *Journal of Geophysical Research: Atmospheres*, **110 (D21)**.

Son, S.-W., E. P. Gerber, J. Perlwitz, L. M. Polvani, and C.-. collaborators, 2010: Impact of stratospheric ozone on Southern Hemisphere circulation change: A multimodel assessment. *Journal of Geophysical Research (Atmospheres)*, **115**, D00M07, doi:10.1029/2010JD014271.

Son, S.-W., A. Purich, H. H. Hendon, B.-M. Kim, and L. M. Polvani, 2013: Improved seasonal forecast using ozone hole variability? *Geophysical Research Letters*, **40 (23)**, 6231–6235.

Son, S.-W., and Coauthors, 2008: The impact of stratospheric ozone recovery on the southern hemisphere westerly jet. *Science*, **320 (5882)**, 1486–1489.

Son, S.-W., and Coauthors, 2018: Tropospheric jet response to antarctic ozone depletion: An update with chemistry-climate model initiative (ccmi) models. *Environmental Research Letters*, **13 (5)**, 054 024.

Stolarski, R. S., A. R. Douglass, M. Gupta, P. A. Newman, S. Pawson, M. R. Schoeberl, and J. E. Nielsen, 2006: An ozone increase in the Antarctic summer stratosphere: A dynamical response to the ozone hole. *Geophys. Res. Lett.*, **33**, L21805, doi:10.1029/2006GL026820.

Sun, L., G. Chen, and W. A. Robinson, 2014: The role of stratospheric polar vortex breakdown in southern hemisphere climate trends. *Journal of the Atmospheric Sciences*, **71 (7)**, 2335–2353.

Thompson, D. W., and J. M. Wallace, 2000: Annular modes in the extratropical circulation. part i: Month-to-month variability. *Journal of climate*, **13 (5)**, 1000–1016.

Thompson, D. W. J., S. Solomon, P. J. Kushner, M. H. England, K. M. Grise, and D. J. Karoly, 2011: Signatures of the Antarctic ozone hole in Southern Hemisphere surface climate change. *Nature Geoscience*, **4**, 741–749, doi:10.1038/ngeo1296.

Trenberth, K. E., and D. P. Stepaniak, 2002: A pathological problem with NCEP reanalysis in the stratosphere. *J. Clim.*

Ummenhofer, C. C., A. S. Gupta, and M. H. England, 2009: Causes of late twentieth-century trends in new zealand precipitation. *Journal of Climate*, **22 (1)**, 3–19.

Watson, P. A., and L. J. Gray, 2015: The stratospheric wintertime response to applied extratropical torques and its relationship with the annular mode. *Climate Dynamics*, **44 (9-10)**, 2513–2537, doi:10.1007/s00382-014-2359-2.

Waugh, D. W., C. Garfinkel, and L. M. Polvani, 2015: Drivers of the recent tropical expansion in the southern hemisphere: Changing ssts or ozone depletion? *J. Clim.*, **28**, 6581–6586, doi:10.1175/JCLI-D-15-0138.1.

Weber, M., M. Coldewey-Egbers, V. E. Fioletov, S. M. Frith, J. D. Wild, J. P. Burrows, C. S. Long, and D. Loyola, 2018: Total ozone trends from 1979 to 2016 derived from five merged observational datasets–the emergence into ozone recovery. *Atmospheric Chemistry and Physics*, **18 (3)**, 2097–2117.

White, I. P., C. I. Garfinkel, E. P. Gerber, M. Jucker, P. Hitchcock, and J. Rao, 2020: The generic nature of the tropospheric response to sudden stratospheric warmings. *Journal of Climate*, **33 (13)**, 5589–5610, doi:10.1175/JCLI-D-19-0697.1.

Wiscombe, W. J., and S. G. Warren, 1980: A model for the spectral albedo of snow. i: Pure snow. *Journal of the Atmospheric Sciences*, **37 (12)**, 2712–2733.

World Meteorological Organization, 2011: *Scientific Assessment of Ozone Depletion: 2010*. Global Ozone Research and Monitoring Project Rep. No. 52, 516 pp.

World Meteorological Organization, 2014: *Scientific Assessment of Ozone Depletion: 2014*. Global Ozone Research and Monitoring Project Rep. No. 55, 416 pp.

Yang, H., L. Sun, and G. Chen, 2015: Separating the mechanisms of transient responses to stratospheric ozone depletion–like cooling in an idealized atmospheric model. *Journal of Atmospheric Sciences*, **72 (2)**, 763–773.

Yang, J., Q. Bao, D. Ji, D. Gong, R. Mao, Z. Zhang, and S.-J. Kim, 2014: Simulation and causes of eastern antarctica surface cooling related to ozone depletion during austral summer in fgoals-s2. *Advances in Atmospheric Sciences*, **31 (5)**, 1147–1156.

Young, P., S. Davis, B. Hassler, S. Solomon, and K. Rosenlof, 2014: Modeling the climate impact of southern hemisphere ozone depletion: The importance of the ozone data set. *Geophysical Research Letters*, **41 (24)**, 9033–9039, doi:10.1002/2014GL061738.